WATER RESOURCES RESEARCH, VOL. 49, 8310–8327, doi:10.1002/2013WR014287, 2013

Hydraulic fracturing in faulted sedimentary basins: Numerical simulation of potential contamination of shallow aquifers over long time scales

Claire Gassiat,[1] Tom Gleeson,[1] René Lefebvre,[2] and Jeffrey McKenzie[3]

Received 17 June 2013; revised 9 October 2013; accepted 23 October 2013; published 12 December 2013.

[1] Hydraulic fracturing, used to economically produce natural gas from shale formations, has raised environmental concerns. The objective of this study is to assess one of the largely unexamined issues, which is the potential for slow contamination of shallow groundwater due to hydraulic fracturing at depth via fluid migration along conductive faults. We compiled publically available data of shale gas basins and hydraulic fracturing operations to develop a two-dimensional, single-phase, multispecies, density-dependent, finite-element numerical groundwater flow and mass transport model. The model simulates hydraulic fracturing in the vicinity of a permeable fault zone in a generic, low-recharge, regional sedimentary basin in which shallow, active groundwater flow occurs above nearly stagnant brine. A sensitivity analysis of contaminant migration along the fault considered basin, fault and hydraulic fracturing parameters. Results show that specific conditions are needed for the slow contamination of a shallow aquifer: a high permeability fault, high overpressure in the shale unit, and hydrofracturing in the upper portion of the shale near the fault. Under such conditions, contaminants from the shale unit reach the shallow aquifer in less than 1000 years following hydraulic fracturing, at concentrations of solutes up to 90% of their initial concentration in the shale, indicating that the impact on groundwater quality could be significant. Important implications of this result are that hydraulic fracturing should not be carried out near potentially conductive faults, and that impacts should be monitored for long timespans. Further work is needed to assess the impact of multiphase flow on contaminant transport along natural preferential pathways.

Citation: Gassiat, C., T. Gleeson, R. Lefebvre, and J. McKenzie (2013), Hydraulic fracturing in faulted sedimentary basins: Numerical simulation of potential contamination of shallow aquifers over long time scales, *Water Resour. Res.*, *49*, 8310–8327, doi:10.1002/2013WR014287.

1. Introduction

[2] Over the past 15 years, shale gas has emerged as a viable and important energy resource. In order to produce economically viable quantities of natural gas from unconventional reservoirs such as shale, the technique of hydraulic fracturing (hydrofracturing or "fracking") is generally used [*BAPE*, 2011; *EPA*, 2012]. Hydraulic fracturing consists of injecting high volumes of "fracturing fluid" at pressures greater than lithostatic, causing the formation to fracture and thereby increase its local permeability [*EPA*, 2012]. After hydraulic fracturing the pressure is relieved by the "flowback," composed of fracture fluid and formation fluids, which returns to the surface [*Gregory et al*., 2001]. The fracking fluid is commonly composed of ~99.5% water and proppants (generally sand), and ~0.5% chemical additives including acids, solvents, and biocides [*BAPE*, 2011; *Gregory et al*., 2011]. Additionally, the flowback not only contains saline formation fluids and natural gas but also naturally occurring contaminants present in the host shale rocks such as radioactive compounds and heavy metals [*Gregory et al*., 2001; *Groundwater Protection Council and All Consulting*, 2009].

[3] Concerns about the potential environmental impact of hydraulic fracturing have increased, especially risks relating to drinking water resources [*Kargbo et al*., 2010; *EPA*, 2012]. Potential drinking water issues include: (1) water resource stress due to water withdrawal; (2) water pollution related to spills and leaks at above ground hydraulic fracturing operations; (3) unsuitable treatment of wastewater; (4) failures of wells in the shallow subsurface due to poor cementing or steel casing corrosion; and (5) geologic failures at depth as a result of the fracturing that could cause potential contamination of

This article was published with an incorrect title on 12 December 2013. This error was corrected on 18 December 2013.

[1]Department of Civil Engineering, McGill University, Montreal, Quebec, Canada.
[2]Institut National de la Recherche Scientifique, Centre Eau Terre Environnement (INRS-ETE), Quebec, Quebec, Canada.
[3]Department of Earth and Planetary Sciences, McGill University, Montreal, Quebec, Canada.

Corresponding author: T. Gleeson, Department of Civil Engineering, McGill University, 817 Sherbrooke St. W., Montreal, QC H3A 0C3, Canada. (tom.gleeson@mcgill.ca)

0043-1397/13/10.1002/2013WR014287

shallow groundwater aquifers via preferential pathways [*EPA*, 2012]. Some of these issues can be addressed by better design and the application of stringent regulations. However, the impact and potential of contamination of groundwater over long time scales aquifers related to the fracturing of the target shale unit is unclear. Although fluid migration rates are usually extremely slow in deep sedimentary systems, heterogeneities such as faults can provide preferential pathways [*Garven*, 1995; *Person et al*., 1996] through which fluids carrying contaminants may migrate more rapidly to reach shallow aquifers.

[4] The potential contamination of shallow aquifers from fluids originating from gas-bearing shales via preferential pathways such as faults has been acknowledged [*BAPE*, 2011; *EPA*, 2012], but is often considered negligible compared to other potential drinking water issues related to shale gas exploitation. This type of contamination has been considered as highly unlikely because (1) no fracking fluid has yet been found in drinking water wells [*Osborn et al*., 2011]; (2) the significant distance between the shale unit (at depths up to a few thousand meters) and the shallow aquifers (at less than a few hundred meters depth) would not lead to contaminant migration over short timescales [*Alpha Environmental Consultants*, 2009; *Zoback et al*., 2010; *BAPE*, 2011; *Howarth et al*., 2011]; (3) the formations above the shale unit often contain low-permeability lithologies that would decrease further the rate of transport [*Arthur et al*., 2008; *BAPE*, 2011]; (4) it is very unlikely that hydraulic fractures would propagate over such long distances to directly connect the gas shale and shallow aquifers [*Zoback et al*., 2010]; (5) fault reactivation due to hydraulic fracturing would likely occur on small distances of a few meters [*EPA*, 2012]; and (6) during gas production, downwards and horizontal flow to the horizontal shale gas well would be promoted, decreasing the risk of upwards migration [*Howarth et al*., 2011].

[5] Conceptually, although fluid migration rates are usually extremely slow in deep sedimentary basins, migration of contaminants from the gas shale driven by an overpressured shale gas formation to a shallow aquifer may be possible if hydraulic fracturing induces communication with other fluid conductive paths, such as faults or production wells. If conductive paths are present from the gas-bearing shale to shallower depths, the long distances and low-permeability units may not act as sufficient barriers for fluid flow to shallow aquifers. Furthermore, although fluid flow toward horizontal shale gas wells would be enhanced during gas production, it may not be the case once production has stopped as overpressure may still remain in the gas shale. Finally, the lack of observed contamination of drinking water wells, after less than 30 years of shale gas hydraulic fracturing, does not preclude future groundwater contamination.

[6] We discern three scenarios in which a hydraulically conductive fault zone could represent a potential pathway for contamination from a hydraulic fracture zone: (1) hydraulic fracturing reactivates a nearby fault zone due to the stress regime in the formation causing additional deformation and offset; (2) hydraulic fractures may develop from the production well to the fault zone, potentially increasing the size or permeability of the damage zone associated with the fault; and (3) the fault zone may act as a hydraulic conduit, even without interaction with hydraulic fractures. Fault zone reactivation and the loss of hydraulic fracturing fluids into fault zones suggest these scenarios are plausible. Fault slippage and reactivation [*Sibson*, 1990; *Zoback*, 2007] is caused by liquid or gas injection [*Streit and Hillis*, 2004; *Soltanzadeh and Hawkes*, 2009; *Konstantinovskaya et al*., 2012], or by the depletion of fluid pressures during production [*Streit and Hillis*, 2004]. Additionally faults are controlled by shear and normal stress components on the fault plane [*Nacht et al*., 2012], fault orientation [*Rudnicki*, 2002; *Soltanzadeh and Hawkes*, 2009], and the reservoir geometry and dip angle [*Soltanzadeh and Hawkes*, 2008]. Fault zone reactivation due to hydraulic fracturing has been reported by several microseismic studies and is one of the most common anomalies identified using microseismic measurements [*Cipolla et al*., 2011]. During hydraulic fracturing operations, faults are generally avoided when drilling as they give rise to a number of problems. The negative impact of fracturing in the vicinity of a fault zone are a decreased hydraulic fracturing of the target formation, a potential increase in flowback water, and a significant cost to the operator in terms of time and materials [*Wessels et al*., 2011]. Several reports underline the issues related to fault zone reactivation in hydraulic fracturing operations [*Soltanzadeh and Hawkes*, 2008; *Maxwell et al*., 2009; *Soltanzadeh and Hawkes*, 2009; *Cipolla et al*., 2011; *Wessels et al*., 2011], suggesting that fracturing in the proximity of permeable fault zones at depth is not an uncommon occurrence.

[7] Although fault zones can clearly be permeable hydraulic features at the typical depth range of prospective shale gas formations (0.5–4.5 km [*EIA*, 2011b]), an important question is whether fault zones could be continuous permeable features from the depth of shale gas formations to near the surface. Fault zones have a complex hydraulic structure that can be barriers, conduits, or conduit-barriers [*Caine et al*., 1996; *Aydin*, 2000; *Rawling et al*., 2001; *Bense and Person*, 2006; *Bense et al.*, 2013]. Techniques for predicting low permeability fault zones in sedimentary basins, called "fault seals" have been described in the petroleum literature. For example, the shale gouge ratio [*Yielding et al*., 1997] uses the estimated clay-content of faults to determine the sealing capacity of the fault. However, multiple lines of evidence suggests faults in sedimentary basins can also be conduits of gas, petroleum, and mineral deposits [*Moretti*, 1998; *Pinti and Marty*, 2000; *Boles et al*., 2004; *Muchez et al*., 2005; *Person et al*., 2008; *Pfaff et al*., 2010]. Mineral deposits, such as Carlin and Mississippi Valley type, located along faults indicate that extensional fault zones have transient permeability fields that are conductive from kilometers depth to shallow depths at least episodically over geologic time [*Muchez et al*., 2005; *Person et al*., 2008; *Pfaff et al*., 2010]. Correlations between noble gas concentrations and geological features suggest the upwards migration of gas and deep fluids through fractures and faults [*Lombardi and Pinti*, 1992]. Hydrocarbon modeling and observation suggests even very narrow, transient, and moderately permeable faults can focus the migration of hydrocarbons [*Moretti*, 1998; *Pinti and Marty*, 2000; *Boles et al*., 2004]. Fault zones in siliciclastic sedimentary basins are often sand-

shale gouges acting as complex conduit-barrier systems with transient fault permeability structures likely evolve on short to geological timescales [*Faulkner et al*., 2010]. The gas, mineral, and petroleum observations, as well as the evidence of fault zone reactivation and the loss of hydrofracturing fluids into fault zones at depth, suggest that some fault zones could be hydraulically conductive from the shale gas formation to shallow depths. For any given basin, actual sedimentary, stress, structural, and hydraulic conditions will have to be assessed to identify the potential presence of hydraulically conductive faults. Previously, a simple groundwater flow and transport model simulated the migration of contaminants from a shale formation to shallow depths through a fault zone [*Myers*, 2012]. However, the conclusions drawn from this model have been questioned because of the simplifications and assumptions of this model including unrealistic boundary conditions and using a constant density, finite-difference, single-phase simulator [*Saiers and Barth*, 2012; *Cohen et al*., 2013]. Thus, there is a need for more realistic modeling of these fault processes for a better understanding of the risks associated with contamination of shallow aquifers due to hydraulic fracturing.

[8] The objective of this study is to assess whether hydraulic fracturing could lead to contamination of shallow aquifers via preferential fluid migration along faults, and what factors control the potential for significant contaminant transport into shallow aquifers. To achieve these objectives we: (1) compiled publically available data on shale gas formations, fault parameters, and hydraulic fracturing operations; (2) used a numerical model to simulate the effect of shale gas fracturing in a generic faulted sedimentary basin that is representative of the data from multiple basins; and (3) conducted a sensitivity analysis with the model to examine the sensitivity of contaminant transport to basin, fault, and hydraulic fracturing parameters that covers the range of parameters found in literature. The numerical model is a two-dimensional, single-phase, multispecies, density-dependent, finite-element numerical groundwater model, and is used to assess the solute transport potential along a fault zone, from a shale formation to a shallow aquifer, following hydraulic fracturing.

2. Generic Model

[9] We systematically reviewed publically available data to develop a generic model representative of shale gas basins (Table 1). Sedimentary basins are layered hydrogeologic systems that are often deformed by multiple cross-cutting fault zones. Prospective shale gas formations are generally at depths of 1–4 km [*EIA*, 2011a] and occur in regions of low to moderate topography. The distance between major regional faults in rift or foreland basins is a few kilometers, such as in the St. Lawrence lowlands where the Utica shale is found [*Séjourné et al*., 2013]. The permeability of shale gas formations is extremely low and these formations are often overpressured, partially due to the low permeability combined with the internal gas generation [*Soltanzadeh and Hawkes*, 2009]. The permeability of the sedimentary rocks overlying the shale gas formations can be low to moderate (10^{-20} to 10^{-13} m^2) [*Gleeson et al*., 2011; *Séjourné et al*., 2013]. In this section, we discuss the basin, fault, and hydraulic fracturing parameters used to develop a generic model.

[10] Although more complex and heterogeneous permeability patterns are common in many sedimentary basins, we simulate a simplified system in order to isolate the mechanisms of transport of contaminants present in fluid migrating along a fault due to hydraulic fracturing. We develop a model of a generic, regional sedimentary basin based on hydrological and geological properties of multiple basins with shale gas formations. Primarily, we gathered information on the Utica shale gas development in the St. Lawrence lowlands, QC, Canada, located between the Yamaska fault and the Logan's Line [*Lavoie et al*., 2008; *BAPE*, 2011; *Rivard et al*., 2012; *Séjourné et al*., 2013] because this was the most readily available to the authors. In addition, wherever possible, we gathered data on other active shale gas formations, primarily the Barnett shale in Texas and Marcellus shale in New York and Pennsylvania [*Montgomery et al*., 2005; *Arthur et al*., 2008; *Lavoie et al*., 2008; *Sumi*, 2008; *EIA*, 2011b; *Davies et al*., 2012]. In general, the data from the St. Lawrence lowlands (such as the depth to shale) is consistent with other areas of shale gas development (Table 1). However, there are differences in the St. Lawrence lowlands compared to other gas shales, such as the low permeability unit overlying the shale gas formation. We examine the sensitivity to basin model parameters within the range indicated in Table 2.

[11] Shale gas formations can be underpressured, at hydrostatic pressure, or overpressured. The Utica shale in the St. Lawrence lowlands, the Barnett shale, and the northern part of the Marcellus formation are overpressured [*Montgomery et al*., 2005; *Lavoie et al*., 2008; *Sumi*, 2008; *Rivard et al*., 2012]. Moreover, ~40% of the prospective areas for shale gas extraction globally are overpressured [*EIA*, 2011a]. Therefore, we simulate a scenario of an overpressured shale formation, under a pressure gradient of 13 kPa/m. If the pressure gradient is lower (either in a less overpressured or underpressured formation), the potential for contaminant migration would decrease. The impact of the pressure gradient in the shale is examined with the sensitivity analysis.

[12] High salinities are common in sedimentary basins and most sedimentary basins are saturated with brine. The transition from shallow fresh groundwater to saline fluids is commonly at a few hundred meters depth [*Globensky*, 1972; *Connolly et al*., 1990; *Kharaka and Thordsen*, 1992; *Björlykke and Gran*, 1994; *Hanor and McIntosh*, 2007]. In North America, salinities up to 500 g/L have been reported at depths less than 4 km [*Kharaka and Thordsen*, 1992]. In the St. Lawrence lowlands, salinities of 175 g/L have been reported in the Trenton group, below the Utica shale, which occurs at depths of 800–2000 m [*Ngoc et al*., 2011]. Higher salinities, due to their effect on water density, reduce the potential for vertical groundwater flow from the shale gas formation to the shallow aquifer.

[13] As discussed above, fault zones can be hydraulic barriers, conduits, or conduit-barriers [*Caine et al*., 1996; *Aydin*, 2000; *Rawling et al*., 2001; *Bense and Person*, 2006]. We simulate a relatively simple scenario of a single fault zone that is a continuous, high permeability conduit from the shale gas formation to the shallow aquifer, as a potential worst-case scenario. If the fault zone is

Table 1. Compilation of Parameter Values Reported in the Literature From Quebec (QC), New York (NY), Texas (TX), Pennsylvania (PA), and Other Regions

Parameter	Range of Values	References
Basin Parameters		
Permeability above shale	Fine-grained sediments: 10^{-17} m^2 Coarse-grained sediments: 10^{-13} m^2	*Gleeson et al*. [2011]
Permeability of shale	10^{-23} to 10^{-17} m^2	*Neuzil* [1994]
	10^{-20} to 10^{-16} m^2	*Freeze and Cherry* [1979]
	10^{-23} to 10^{-20} m^2	*Flewelling and Sharma* [2013]
	Utica (QC): 9×10^{-23} to 8×10^{-17} m^2	*Séjourné et al*. [2013]
	Marcellus (NY, PA): 2×10^{-16} m^2	*Soeder* [1988]
	Barnett (TX): $<10^{-17}$ m^2	*Montgomery et al*. [2005]
Porosity above shale	Sandstone: 5–30%	*Freeze and Cherry* [1979]
	Shale: <10%	
	Utica (QC): 1.2–3.2%	*Rivard et al*. [2012]
Porosity of shale	5–60% at 0.3–10 km depth	*Neuzil* [1994]
	<10%	*Freeze and Cherry* [1979]
	US: 1–12%, median: 7%	*EIA* [2011b]
	Utica (QC): 0.7–6.6%	*Lavoie et al*. [2008], *BAPE* [2011], *Rivard et al*. [2012], and *Séjourné et al*. [2013]
	Marcellus (NY, PA): 8%	*EIA* [2011b]
	Barnett (TX): 5%	*EIA* [2011b]
Topographic gradient	St. Lawrence lowlands (Utica): 2.3 ± 2.7% Appalachian basin (Marcellus): 2.5 ± 2.9% Fort Worth basin (Barnett): 1.0 ± 0.7%	
Matrix compressibility	Jointed rock: 10^{-10} to 10^{-8} Pa^{-1} Sound rock: 10^{-11} to 10^{-9} Pa^{-1}	*Freeze and Cherry* [1979]
Pressure gradient in shale	Utica (QC): 10–17 kPa/m	*Lavoie et al*. [2008], *BAPE* [2011], *Rivard et al*. [2012], and *Séjourné et al*. [2013]
	Marcellus (NY, PA): northern basin overpressured	*Sumi* [2008]
	Barnett (TX): 10.4–11.8 kPa/m	*Montgomery et al*. [2005] and *Lavoie et al*. [2008]
	World[a]: 40% overpressured	*EIA* [2011a]
Depth to saline formations	North America: 0–2 km	*Kharaka and Thordsen*. [1992]
	Utica (QC)[b]: 86–1554 m	*Séjourné et al*. [2013]
	Utica (QC): 150–740 m	*Globensky* [1972]
Salinity	North America: 0–500 g/L	*Kharaka and Thordsen*. [1992]
	Utica (QC), shallow depths: 5–225 g/L	*Globensky* [1972]
	Utica (QC), high depths[c]: 100–240 g/L	*Ngoc et al*. [2011]
Depth to shale gas formation	World: 1–4.5 km, average: 2.9 km	*EIA* [2011a]
	US: 0.5–4.5 km, average: 2.3 km	*EIA* [2011b]
	Utica (QC)[d]: 1.2–2.5 km	*BAPE* [2011]
	Marcellus (NY, PA)[e]: 1.2–2.6 km	*Arthur et al*. [2008]
	Barnett (TX): 1.9–2.6 km, average: 2.3 km	*Arthur et al*. [2008] and *EIA* [2011b]
Thickness of shale gas formation	World: 20–300 m, average: 77 m	*EIA* [2011a]
	US: 7–940 m, average: 190 m	*EIA* [2011b]
	Utica (QC): 220 m on average	*BAPE* [2011]
	Marcellus (NY, PA): 15 to 60 m	*Arthur et al*. [2008]
	Barnett (TX): 30–280 m, average: 91 m	*Arthur et al*. [2008] and *EIA* [2011b]
Fault Parameters		
Distance between faults	Utica (QC): 0.6–27.7 km, average: 6.6 km	*Séjourné et al*. [2013]
Hydraulic Fracturing (HF) Parameters		
Length of hydrofracturing zone	1–3 km	*Rivard et al*. [2012]
	1.2 km	*Zoback et al*. [2010]
Vertical extent of hydraulic fractures	100–300 m	*Rivard et al*. [2012]
	Barnett (TX): 46 m above and 61 m below the wellbore	*Zoback et al*. [2010]
	Barnett (TX): <588 m	*Davies et al*. [2012]
	Marcellus (NY, PA): <536 m	
	Most <90 m	*King* [2012]
Permeability of hydrofracturing zone	100–1000 times the permeability of the formation	*King* [2012]

[a]Potential shale gas development in 48 countries.
[b]Saline water index. The interval between the fresh water and saline water index is often of a few hundred meters, which does not allow to accurately locate the transition between fresh water and brine.
[c]Formations below the Utica shale (Postdam and Beekmantown groups).
[d]Only the area of interest for shale gas development, between the Yamaska fault and the Logan Line, has been considered.
[e]Marcellus shale targeted for exploitation.

Table 2. Parameter Values Used in the Base Case Model and Range of Variation for Sensitivity Analysis

Parameter	Base Case Value	Range of Variation for Sensitivity Analysis
Basin Parameters		
Permeability above shale (m^2)	10^{-15}	10^{-18} to 10^{-13}
Porosity above shale	0.03	0.01–0.1
Topographic gradient	0.002	0.0004–0.01
Matrix compressibility (Pa^{-1})	10^{-8}	10^{-9} to 10^{-7}
Overpressure in shale (kPa/m)	13	9–25
Fault Parameters		
Permeability of fault above shale (m^2)	10^{-13}	10^{-15} to 10^{-11}
Permeability of fault in shale (m^2)	10^{-18}	10^{-20} to 10^{-16}
Fault anisotropy above shale	1	1–1000
Fault anisotropy in shale	1	1–1000
Fault orientation relative to horizontal α (°)	135	30–150
Hydraulic Fracturing (HF) Parameters		
Permeability of HF zone (m^2)	10^{-17}	10^{-19} to 10^{-15}
Distance from HF zone to fault zone (m)	0	0–1000
Thickness of shale above HF zone (m)	25	0–50
Length of HF zone (km)	2	1–3
Thickness of HF zone (m)	150	60–200

more of a barrier (either continuously or at specific depths), the potential for transport through the fault would be reduced or potentially negligible. We simulate the effect of reducing fault permeability as well as the case of conduit-barrier by changing the anisotropy (the ratio of permeability along fault to permeability perpendicular to fault) instead of simulating a discrete low permeability fault core flanked by a high permeability damage zone [*Caine et al*., 1996].

[14] In hydrofracturing operations, a horizontal well is drilled within the shale formations for a length of a few kilometers and hydraulic fracturing is performed in stages at intervals of tens of meters [*Zoback et al*., 2010]. Hydraulic fractures can extend up to a few hundred meters above and below the horizontal wellbore [*Zoback et al*., 2010; *Davies et al*., 2012; *King*, 2012] and can increase the permeability of the formation up to three orders of magnitude [*King*, 2012]. The shale gas formations are generally thin (less than 100 m in most major U.S. shale gas development) [*EIA*, 2011b], especially in comparison to the thickness that is typically affected by hydraulic fracturing. The goal of hydraulic fracturing is to develop the maximum contact with the producing formation, while minimizing fracturing of formations above or below which can lead to additional costs in terms of fracking fluid, pressure loss, and time [*King*, 2012]. Therefore, we assume that hydrofractured zones can extend to the top of the shale gas formation. We do not simulate the actual geomechanical deformation of hydraulic fracturing but rather the impact of increased permeability due to hydraulic fracturing. We focus on the period after hydraulic fracturing because the pressure pulse of hydraulic fracturing would rapidly decay and would not have a significant impact on the migration of contaminants over long time scales, which is the focus of the present study. For ductilely deformed shale formations, permeability from hydrofracturing may be temporally reduced on decadal timescales, which would reduce contamination potential.

3. Numerical Methods and Parameter Values

[15] Simulations were conducted with SUTRA-MS, a US Geological Survey numerical variable-density simulator of groundwater flow as well as the transport of multiple-solutes [*Voss and Provost*, 2002; *Hughes and Sanford*, 2005]. The base case value of each parameter of interest and its range of variation in the sensitivity analysis are presented in Table 2 and other properties used for all simulations are presented in Table 3. The model domain consists of a vertical cross-section of a 50 km long, 2 km deep portion of a sedimentary basin (Figure 1) with a linear topographic gradient. To simulate the type of nested, active groundwater flow that occurs in undulating topography [*Tóth*, 1963], we imposed five recharge areas at the upper boundary, alternating with six specified pressure boundaries ($P = 0$) which represent discharge areas such as surface water bodies. The lateral sides and base of the model domain are no-flow boundaries. Permeability and thickness of the shallow aquifer were assigned based on field data from the St. Lawrence lowlands and the recharge rate was adjusted in order to result in a realistic depth of the active flow zone (Table 2). A 3.5 mm/year value of recharge was chosen so that the active flow zone is limited to approximately the first 200 m below the surface for the permeability and geometry of the 100 m thick shallow aquifer. Although this is a lower recharge rate than expected in the St. Lawrence lowlands, this study focuses on deep groundwater flow from the shale unit to shallow aquifers, and a modification of the recharge rate would not impact the results in terms of solute mass fluxes reaching the freshwater aquifer, although the concentrations of these solutes

Table 3. Parameters Used in All Simulations

Parameter	Value
Liquid Water	
Fluid compressibility ($(m \cdot s^2)/kg$)	4.47×10^{-10}
Fluid viscosity ($kg/(m \cdot s)$)	1.0×10^{-3}
Initial salt concentration below 200 m (kg/m^3)	100
Solid Matrix	
Solid matrix compressibility ($(kg/(m \cdot s^2))^{-1}$)	1.0×10^{-8}
Density of solid grains (kg/m^3)	2650
Porosity in the upper layer	0.3
Porosity in the middle and shale layers	0.03
Permeability in the upper layer (m^2)	1×10^{-13}
Permeability in the middle layer (m^2)	1×10^{-15}
Permeability in the shale layer	1×10^{-20}
Basin anisotropy k_x/k_z	100
Other	
Gravity (m/s^2)	−9.81
Longitudinal dispersivity (m)	10
Transverse dispersivity (m)	1
Transport	
Molecular diffusivity of solutes in pure fluid (m^2/s)	1.0×10^{-9}
Fluid base density (kg/m^3)	1000
Coefficient of fluid density change with concentration of salt ($kg^2/(m^3 \cdot kg)$)	700
Coefficient of fluid density change with concentration of tracers ($kg^2/(m^3 \cdot kg)$)	0
Upper Boundary	
Fluid source rate at recharge nodes (mm/yr)	3.5

in the aquifer would be lower if more important recharge and groundwater flow occurred in the freshwater aquifer.

[16] The basin contains three layers (Figure 1): (1) a 200 m thick, low permeability unit at the base of the model domain representing the shale gas unit; (2) a relatively permeable bedrock layer overlying the shale; and (3) a highly permeable, 100 m thick layer at the top of the basin representing a shallow unconsolidated aquifer. Depths and thicknesses of the different units were derived based on the St. Lawrence lowlands (structural corridor C of *Séjourné et al*. [2013]) and are representative of typical basins with shale gas extraction. Each unit is assumed to be homogeneous and anisotropic ($k_x/k_z = 100$). Permeabilities and porosities of the three units were derived from data and literature values of the St. Lawrence lowlands. We assigned the permeability of the shale unit at 10^{-20} m^2 by considering (1) the usual range of shale permeability (Table 1); (2) the relationship of permeability with depth usually observed [*Ingebritsen et al*., 2006]; and (3) the capacity to maintain overpressure over geological time scales.

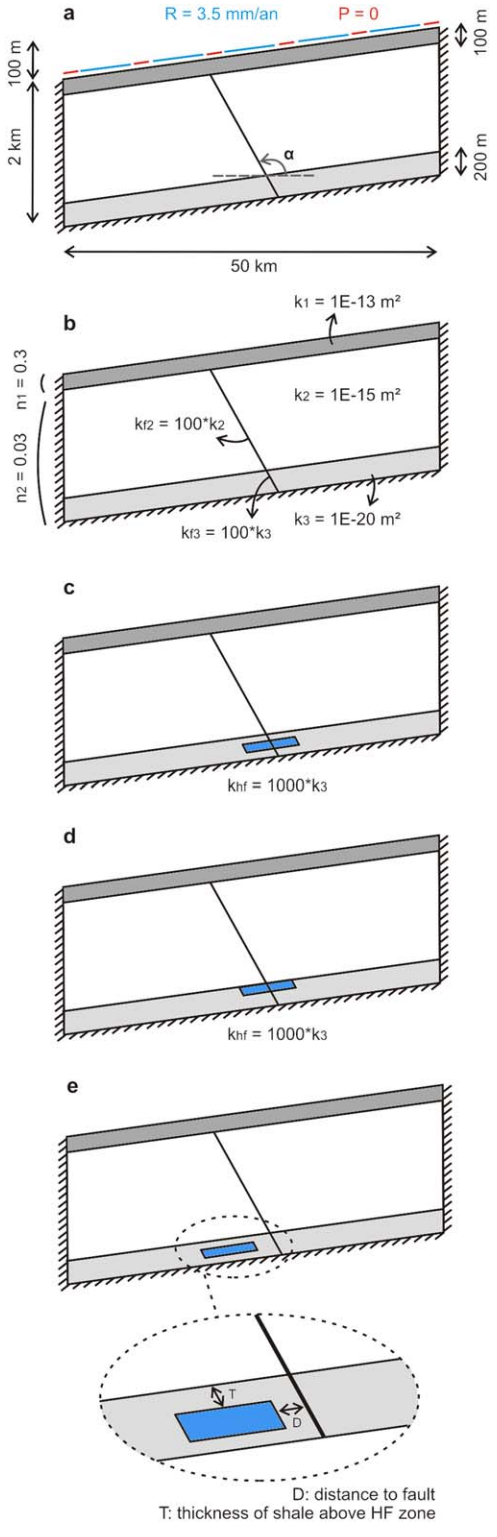

Figure 1.

[17] A 10 m wide, continuous normal fault zone is located in the middle of the model domain, and crosscuts the entire thickness of the bedrock but not the shallow, unconsolidated aquifer (Figure 1). This fault thickness is consistent with a regional fault with hundreds of meters of displacement [*Childs et al*., 2009]. An isotropic permeability of two orders of magnitude higher than the permeability of the surrounding material is assigned to the fault zone. Fault anisotropy, defined as the ratio of permeability along fault to permeability perpendicular to fault, is studied in the sensitivity analysis. In the sensitivity analysis of the anisotropy ratio, permeability along fault is left unchanged while permeability perpendicular to fault is reduced.

[18] Considering a single fault zone is consistent with the fault density in the St. Lawrence lowlands and the purpose of the study. The spatial density of major faults in the St. Lawrence lowlands (Table 1) suggests that a single horizontal well would not likely cross more than one fault zone [*Séjourné et al*., 2013]. The purpose of the simulations is a process-based understanding of contaminant transport potential, and not on the estimation of the total cumulative fluxes of contaminants that could migrate along faults due to regional-scale hydraulic fracturing of a gas shale unit.

[19] The shale is considered overpressured, with a pressure gradient of 13 kPa/m [*Lavoie et al*., 2008; *Rivard et al*., 2012; *Séjourné et al*., 2013], which corresponds to an overpressure of 6 MPa at 1.9 km depth (Figure 2). Brine has been observed at a few meters to a few hundred meters depth in the St. Lawrence lowlands [*Séjourné et al*., 2013],

Figure 1. General setup of the numerical model (not to scale): (a) model domain and boundary conditions. R stands for recharge and P is pressure relative to atmospheric conditions. The angle α measures the fault orientation relative to horizontal; (b) permeability and porosity of the different units; (c) base case scenario with hydraulic fracturing in the middle of the shale; and (d) base case scenario with hydraulic fracturing at the top of the shale. Hydraulic fracturing is modeled by an increase of permeability in the hydraulic fracturing zone (in blue). In the base case, the hydraulic fracturing zone crosses the fault zone; (e) scenario where the hydraulic fracturing zone does not cross the fault zone. T is the thickness of shale above HF zone and D is the distance of hydraulic fracturing (HF) zone to fault zone.

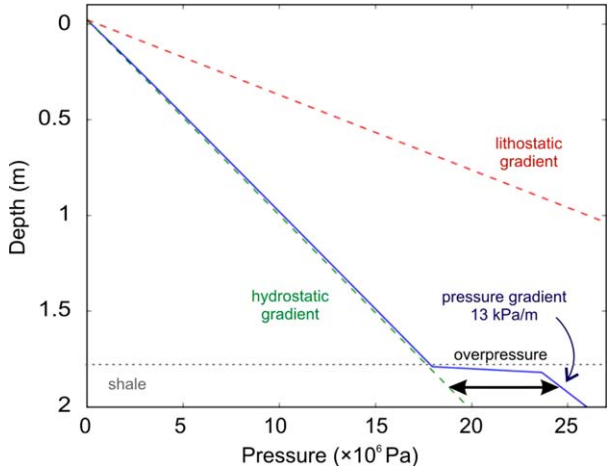

Figure 2. Initial pressure variation with depth at $x = 10$ km. A pressure gradient in the shale of 13 kPa/m corresponds to an overpressure of 6 MPa in the middle of the shale at 1900 m depth.

and high salinities of 175 g/L have been reported in the Trenton group, below the Utica shale [*Ngoc et al.*, 2011]. Therefore, the concentration of brine was assigned as 100 g/L below 200 m depth. As a comparison, water is often considered as nonsaline when the concentration of salt is below 4 g/L [*BAPE*, 2011]. Hydraulic fracturing was simulated by increasing the permeability of a 2 km long, 150 m thick zone in the vicinity of the fault. Two base case scenarios were simulated, with the hydraulic fracturing zone located either in the middle of the shale unit (Figure 1c) or at the top of the shale unit (Figure 1d) since the width of the hydrofracturing zone relative to the thickness of shale gas formations suggests this is likely common. In both scenarios, the hydrofractured zone crosses the fault. In the sensitivity analysis, we laterally moved the hydraulically fractured zone away from the fault.

[20] The 46,060 element numerical mesh is shown in Figure 3. Grid spacing telescopes from 1 m × 10 m finite elements (vertical × horizontal extent) in the fault zone to 200 m × 30 m elements in regions most distal from the fault. Horizontal discretization is 1 m for elements in the

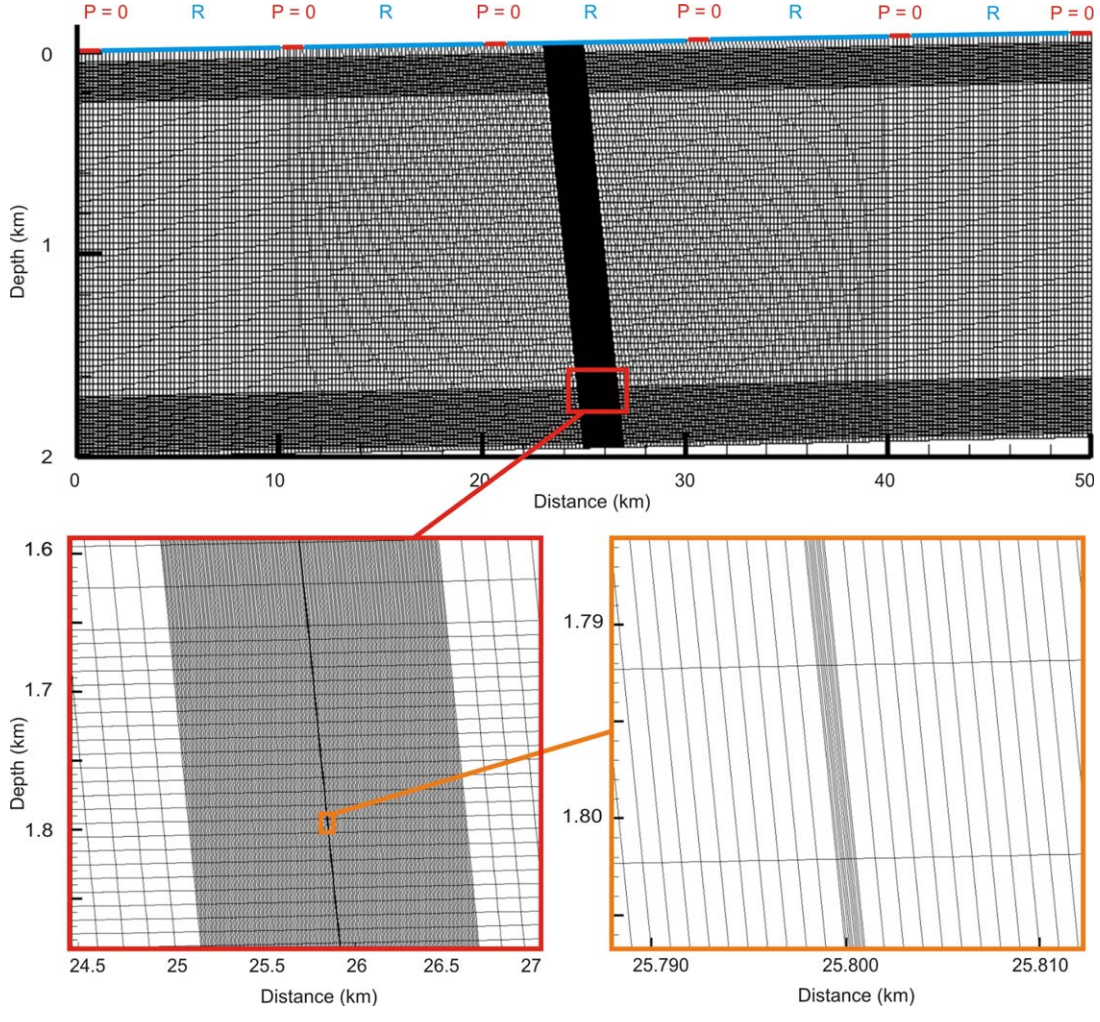

Figure 3. Finite-elements mesh used for the numerical simulation. (top) Five recharge areas (R, in blue) were imposed at the upper boundary, alternating with six specified pressure boundaries ($P = 0$, in red) which represent discharge areas. The lateral sides and base of the model domain are no-flow boundaries.

fault zone, 10 m for elements within 1 km of the fault zone, and 200 m for elements at greater distances. Vertical discretization is 10 m in the upper (20–200 m depth) and lower (1700–2000 m depth) parts of the model domain and 30 m in between. Doubling the grid refinement showed that results were not sensitive to grid resolution. At each time step, the flow and transport equations were solved using Gaussian elimination [*Voss and Provost*, 2002].

[21] Simulations were conducted in two consecutive runs. An initial 300,000 year run was used to reach steady-state pressure and solute conditions. In this initial run, the pressure gradient in the shale is specified and the brine concentration below 200 m depth is also specified. The output from this run was used as initial conditions for a second run, in which pressure and concentration are not specified [*Saiers and Barth*, 2012; *Cohen et al*., 2013]. This second simulation was run over 100,000 years to assess whether the pressure field and the concentration field were stable. The dissipation of the pressure gradient within the shale was negligible over 100,000 years when the permeability in the shale unit was 10^{-20} m^2. A 5000 year period in the middle of the second simulation was thus selected as the time examined ($t = 0 - 5000$ years) to assess potential contamination for hydrofracturing scenarios (by modifying permeability of the hydrofractured zone at $t = 0$ years) or without hydrofracturing. The initial hydraulic head distribution and concentration field at $t = 0$ years are presented in Figures 4a and 4b. For each simulation, initial time-step size was set at 1 year. Time-step size was incremented by a factor of 1.5 every 10 time steps until the maximum time step size of 10 years is reached. Reducing the time step showed that results were not sensitive to the time steps used.

[22] Three passive tracers were simulated in order to study the movement in regional groundwater flow due to hydraulic fracturing (Figure 4). At $t = 0$, the first tracer, herein called the "shale tracer" is located in the shale layer ($-2000 < z < -1800$); the second tracer, herein called the "lower basin tracer," is located in the lower part of the overlying unit ($-1800 < z < -1000$); and the third tracer, herein call the "upper basin tracer," is located in the upper part of the overlying unit ($-1000 < z < -200$) up to the fresh water aquifer. We define the depth of potential contamination as the shallowest depth relative to the land surface where the concentration of the shale tracer is above 1% of its initial concentration in shale. The shale tracer represents any potential contaminant originating from the shale unit: chemicals in fracking fluid initially after fracturing, or naturally occurring contaminants in the shale such as radioactive materials or heavy metals for the entire duration of simulations. The value of 1% of initial concentration is arbitrary; other cut offs such as 10% of initial concentration were also examined, and show a similar behavior in sensitivity analysis as discussed below. We compiled the mass fluxes of the three tracers at the top of the fault (i.e., at the base of the shallow freshwater aquifer). We assumed that the initial concentration of TDS in the shale and lower basin was 100 kg/m^3 and calculated the sum of fluxes from the shale and the lower basin in order to estimate the total mass flux of potential contaminants in the shallow aquifer. The upper basin tracer was not considered as there is no clear influence of hydraulic fracturing on its migration.

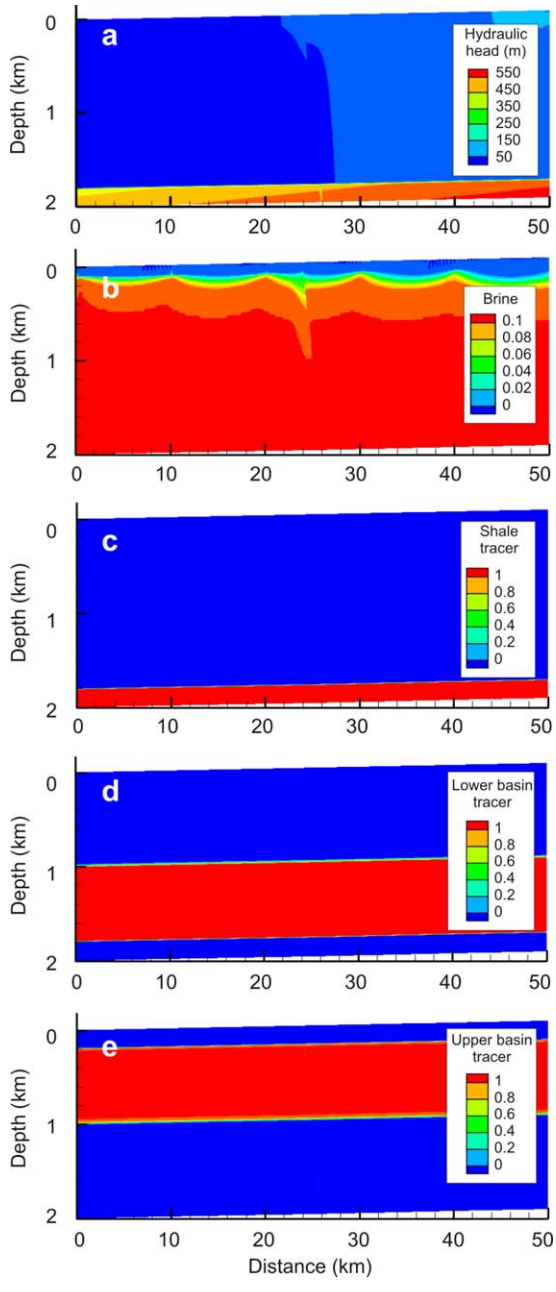

Figure 4. Initial conditions of the base case scenario: (a) initial hydraulic head distribution. In the base case scenario, the shale is overpressured; (b) initial concentration of brine; (c) initial concentration of the shale tracer; (d) initial concentration of the lower basin tracer; and (e) initial concentration of the upper basin tracer.

4. Results

[23] Figure 5 compares the simulated spatial distribution of the shale tracer for the case without hydraulic fracturing (Figure 5a), for the base case scenario with hydraulic fracturing in the middle of the gas shale (Figure 5b), and for the base case scenario with hydraulic fracturing at the top of the gas shale (Figure 5c). No shale tracer migration occurs along the fault without hydraulic fracturing (Figure 5a). For the base case scenarios, shale tracers move up the fault after hydraulic fracturing (Figures 5b and 5c). The

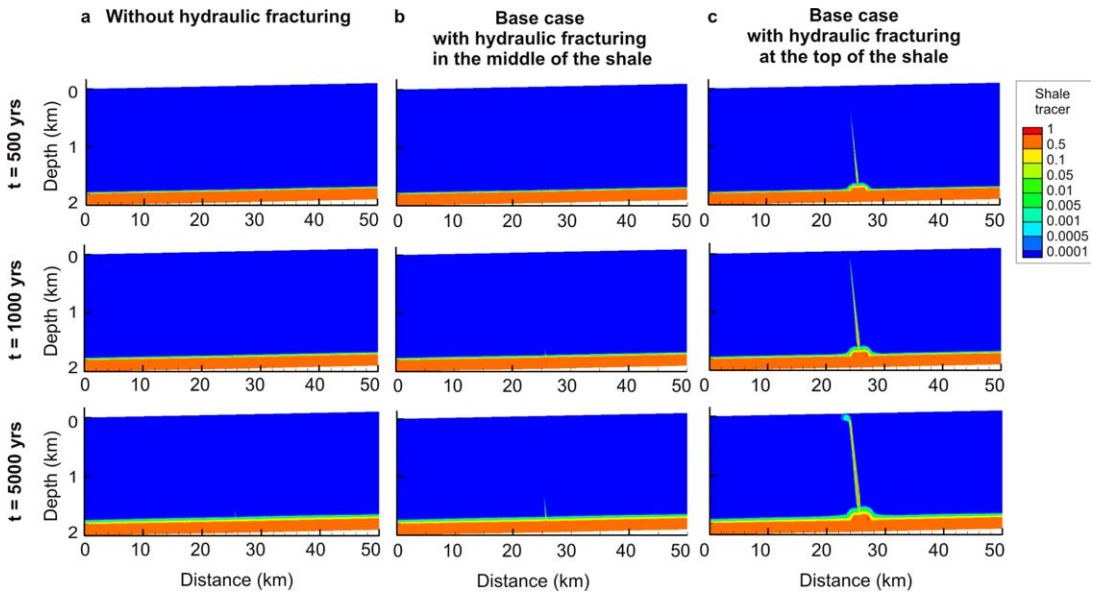

Figure 5. Migration of shale tracer through time: (a) without hydraulic fracturing; (b) with hydraulic fracturing in the middle of the gas shale (first base case scenario); and (c) with hydraulic fracturing at the top of the gas shale (second base case scenario).

base case with hydraulic fracturing in the middle of the shale formation leads to slow migration, which is indicated by the 1% concentration threshold reaching only 1500 m depth at simulation time of 5000 years (apparent on the lower graph of Figure 5b). With hydraulic fracturing at the top of the shale gas formation (Figure 5c), the 1% concentration threshold reaches 500 m depth after about 500 years and the upper part of the fault after about 1000 years. After 5000 years, a plume of shale tracer reaches the shallow aquifer with concentrations up to 5% of the initial tracer concentration in shale. Therefore, in this scenario, the shallow aquifer is significantly contaminated by the tracer from the shale formation. Figure 6 shows the extent and relative concentration of the shale tracer (Figure 6a) and the lower basin tracer (Figure 6b) in the active freshwater flow zone at $t = 5000$ years in the base case scenario with hydraulic fracturing at the top of the shale (lower graph of Figure 5c). The lateral plume of concentrations of shale tracer higher than 0.01 (1%) in the active zone is 500 m, and the extent of concentrations higher than 0.001 (0.1%) is 1.2 km (Figure 6a). The plume with concentrations of shale tracer higher than 0.01 (1%) in the active zone is 300 m, and the extent of concentrations higher than 0.001 (0.1%) is 1 km (Figure 6b). Maximum concentrations of the shale tracer and lower basin tracer in the shallow aquifer are ~5%.

[24] For the base case simulations, Figure 7 shows the migration through time of the three tracers (Figure 4), without hydraulic fracturing or with hydraulic fracturing either in the middle of the shale (Figures 7a and 7c) or at the top of the shale (Figures 7b and 7d). Figure 7 compares tracer migration through time with or without hydraulic fracturing (Figures 7a and 7b), and for thresholds of 1% and 10% of initial concentration (Figures 7c and 7d). The shale tracer, which is initially in the shale, migrates higher upwards when there is hydraulic fracturing in the middle of the shale than without, 300 m compared to 100 m over 5000 years (Figure 7a). The lower basin tracer also moves up the fault, which is consistent with flow in the overlying unit being more significant than in the shale. However, the importance of this migration is quite similar with or without hydraulic fracturing; about 400 m upwards (Figure 7a). The difference in migration of the shale tracer between the case with hydraulic fracturing than without is a lot more apparent when the hydraulic fracturing occurs at the top of the fault, 1700 m compared to 50 m over 1500 years (Figure 7b). In this case, migration of the lower basin tracer is also more important with hydraulic fracturing than without, 900 m compared to 200 m over 1500 years. There is no clear influence of hydraulic fracturing on the migration of the upper basin tracer, which mimics the spatial distribution of solutes in the upper part of the overlying aquifer unit due to active fresh groundwater flow (Figures 7a and 7b). The depths of 1% and 10% concentration thresholds through time have the same pattern (Figures 7c and 7d), so we use a concentration of 1% as the cutoff for the remainder of the analysis. The lower elevation of the 10% concentration, compared to the 1% concentration, is indicative of dispersive effect on the transport of the tracer, either within the fault or due to the exchange of fluid with units adjacent to the fault. The following sections focus on the migration of the shale tracer, from the shale unit, as the potential impact of hydraulic fracturing on groundwater quality in the shallow aquifer is expected to be more related to fluids originating from the shale horizon.

[25] Sensitivity analysis of a variety of basin, fault, and hydraulic fracturing parameters shows that only a few parameters control contaminant migration potential from the gas shale to the shallow aquifer following hydraulic fracturing in the middle of the shale (Figure 8). First, the impact of the following basin parameters were analyzed (Figures 8a, 8d, 8g, 8j, and 8m): pressure gradient in shale, permeability of the unit overlying the shale, topographic

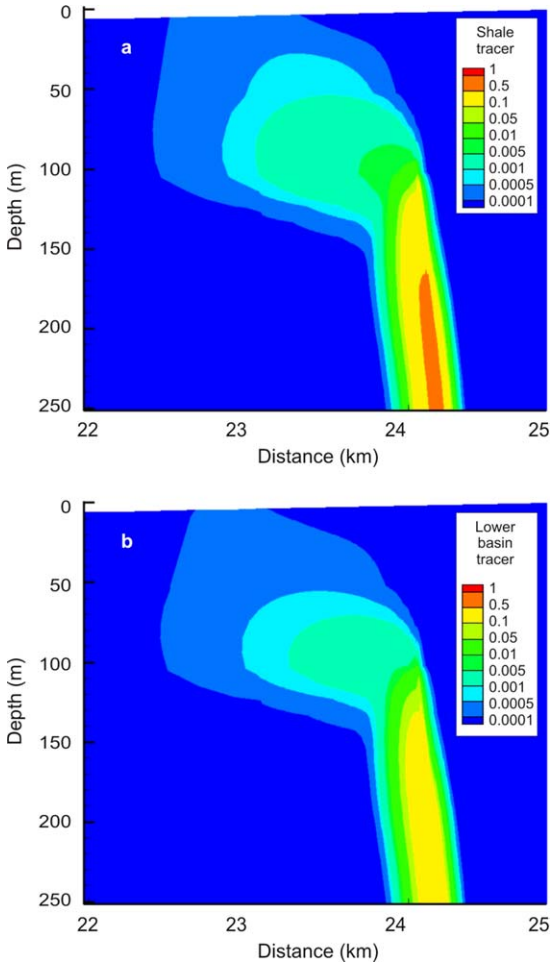

Figure 6. Extent of contamination in the shallow aquifer. Concentration of (a) shale tracer and (b) lower basin tracer in the shallow aquifer at $t = 5000$ years for the base case scenario with hydraulic fracturing at the top of the fault.

gradient, matrix compressibility, and porosity of the unit overlying the shale. The simulation results indicate that the only sensitive basin parameter is the pressure gradient in the shale. Depth of potential contamination decreases systematically with an increase of the pressure gradient in the shale (Figure 8a) as upward flow is driven by the overpressure in the shale. Pressure gradients above 13 kPa/m (overpressure in the middle of the shale above 6 MPa) lead to contamination above 1500 m depth within 5000 years. The other basin parameters have a limited impact on potential contamination indicated by a shale tracer relative concentration of 1% for the model conditions of the base case.

[26] Second, various fault parameters were examined (Figures 8b, 8e, 8h, 8k, and 8n): fault permeability in the unit overlying the shale, fault permeability in shale, fault dip, fault anisotropy in the unit overlying the shale, and fault anisotropy in shale. The simulations show that fault permeability in the shale is the most important parameter, with a higher permeability in the fault resulting in faster migration (Figure 8e). Fault permeability above 10^{-17} m^2 leads to contamination above 1000 m depth within 5000 years. All other fault parameters studied have a limited impact on potential contamination for the base case model conditions.

[27] Third, the effect of hydraulic fracturing parameters was studied (Figures 8c, 8f, 8i, 8l, and 8o): hydrofracturing (HF) zone permeability, distance of the hydrofracturing zone to fault, thickness of shale above the hydrofracturing zone, length of hydrofracturing zone, and thickness of hydrofracturing zone. The depth of potential contamination varies greatly depending on the thickness of shale above the hydrofracturing zone (Figure 8i). Migration of solutes is very slow if the thickness of shale above the hydrofracturing zone is more than 20 m, whereas it is fast when the thickness of shale above the fractured zone is less than 20 m because fluids from the shale travel to the fault through the overlying formation as well as through the hydrofractured zone of the shale formation. In our simulations, the thickness of shale above the hydrofracturing zone appears as the most important parameter controlling the migration along the fault. The other hydraulic fracturing parameters have a limited impact on potential contamination. In summary, when hydraulic fracturing occurs in the middle of the shale, the most important parameters controlling contaminant transport potential are parameters that control migration to the fault in the overlying unit: pressure gradient in shale, fault permeability in shale, and thickness of shale above hydrofracturing zone.

[28] Another set of sensitivity analysis with the same basin, fault, and hydraulic fracturing parameters was conducted with the hydraulic fracturing zone at the top of the shale unit (Figure 9). Overall, the contamination migration is faster and reaches shallower depths at greater concentrations, in part due to rapid transport through the overlying formation. The most sensitive basin parameters (Figures 9a, 9d, 9g, 9j, and 9m) are the pressure gradient in the shale and the permeability of the overlying unit. The speed of migration along the fault increases with the overpressure in shale, and contamination of shallow aquifers is likely to occur as a result of overpressured shales only (pressure gradient in shale $>$ 10 kPa/m) (Figure 9a). A decrease in permeability of the overlying unit leads to slower migration along the fault (Figure 9d). Conversely, potential contamination is largely insensitive to the topographic gradient. The most crucial fault parameter (Figures 9b, 9e, 9h, 9k, and 9n) is fault permeability in the overlying unit (Figure 9b). The change in depth of contamination through time is negligible over the studied variations of fault permeability in shale, fault dip, fault anisotropy in the overlying unit, and in shale (Figures 9e, 9h, 9k, and 9n). Finally, some hydraulic fracturing parameters have an impact on potential contamination (Figures 9c, 9f, 9i, 9l, and 9o). Speed of migration along the fault increases with increasing values of the hydraulic fracturing zone permeability (Figure 9c). Potential contamination occurs at shallower depth when the hydraulic fracturing zone is close to the fault zone (Figure 9f). Length and thickness of the hydraulic fracturing zone have a limited impact on potential contamination (Figures 9l and 9o). In this case, the thickness of shale above the hydraulic fracturing zone appears as the most important parameter controlling the migration along the fault (Figure 9i).

[29] Figure 10 shows the concentration of shale tracer and lower basin tracer at the top of the fault and base of the shallow aquifer following hydraulic fracturing at the top of the fault for several values of pressure gradient in the shale, porosity above shale, fault permeability above shale, fault

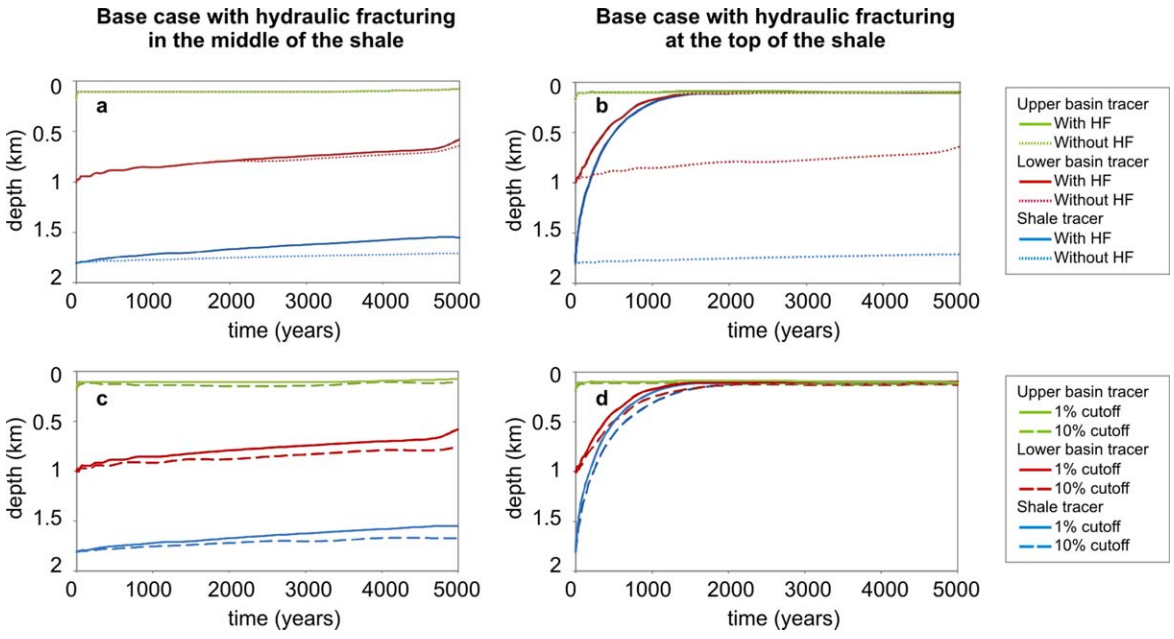

Figure 7. Depth from the land surface of potential contamination from the three tracers through time for the base case with hydraulic fracturing (HF) in (a and c) the middle or (b and d) at the top of the shale gas formations. With and without hydraulic fracturing, with a 1% concentration threshold: (a) with hydraulic fracturing in the middle of the shale and (b) with hydraulic fracturing at the top of the shale. With hydraulic fracturing with a 1% and 10% thresholds: (c) with hydraulic fracturing in the middle of the shale and (d) with hydraulic fracturing at the top of the shale.

orientation, and hydrofractured zone permeability. Concentration of the shale tracer at the top of the fault is 0.01 at 5000 years under a shale pressure gradient of 13 kPa/m (overpressure of 6 MPa in the middle of the shale), and greatly increases under pressure gradients above 15 kPa/m (overpressure of 10 MPa in the middle of the shale) with concentrations up to 0.9 at 5000 years (Figure 10a). Concentrations of the lower basin tracer are slightly lower (Figure 10c), with a maximum concentration of 0.1 at the top of the fault at 5000 years under a pressure gradient in the shale of 16 kPa/m (overpressure of 12 MPa in the middle of the shale). Concentrations of lower basin tracer decrease under pressure gradients above 16 kPa/m. This could be due to the fact that more fluid migrates along the fault as the pressure gradient in shale increases, which includes fluids from the shale and the lower basin up to a pressure gradient of 16 kPa/m. Above that value, the migration of fluids from the shale unit is so dominant that fluids from the overlying unit enter the fault to a lesser degree. Other parameters such as the fault permeability in the overlying unit and the fault orientation also have an impact on the concentrations of tracers at the base of the shallow aquifer following hydraulic fracturing at the top of the shale. If the fault zone has a very high permeability ($\sim 10^{-11}$ m^2) concentrations of both the shale tracer and the lower basin tracer reach 0.3 at 5000 years (Figures 10e and 10f). A vertical fault zone leads to a concentration of shale tracer of 0.2 and a concentration of lower basin tracer of almost 0.1 at 5000 years (Figures 10g and 10h). Variations of other variables do not lead to high concentrations being transported (Figure 10).

[30] We also compute mass fluxes at the top of the fault (i.e., at the base of the shallow aquifer) by assuming that the initial concentration of TDS in the shale and lower basin was 100 kg/m^3. Figure 11a shows the potential sum of fluxes from the shale and the lower basin through time for the scenarios without hydraulic fracturing and for the base cases with hydraulic fracturing in the middle of the shale or at the top of the shale. Fluxes reach 180 g/yr/m following hydraulic fracturing at the top of the shale. Figure 11b shows the potential sum of fluxes from the shale and the lower basin under several pressure gradients in the shale following hydraulic fracturing at the top of the shale. Fluxes reach 3×10^4 g/yr/m under high pressure gradients.

5. Discussion

[31] While it is often considered that fluid migration via natural preferential pathways carrying contamination from a gas shale unit to a shallow aquifer due to hydraulic fracturing is very unlikely [*Arthur et al*., 2008; *Zoback et al*., 2010; *BAPE*, 2011; *Howarth et al*., 2011; *Osborn et al*., 2011; *EPA*, 2012], the simulation results presented in this paper show that the migration of fluids and contaminants over long time scales along a fault zone to shallow aquifers can occur under certain conditions. This study considers the scenario of contamination of shallow aquifers due to migration of contaminants from the shale formation along a fault zone. This scenario is one of many that may lead to groundwater contamination due to shale gas development. Other scenarios, such as groundwater pollution due to spills and leaks at above ground hydraulic fracturing operations, or failures of wells at shallow depth due to poor cementing or steel casing corrosion, could cause contamination of groundwater resources on shorter timescales.

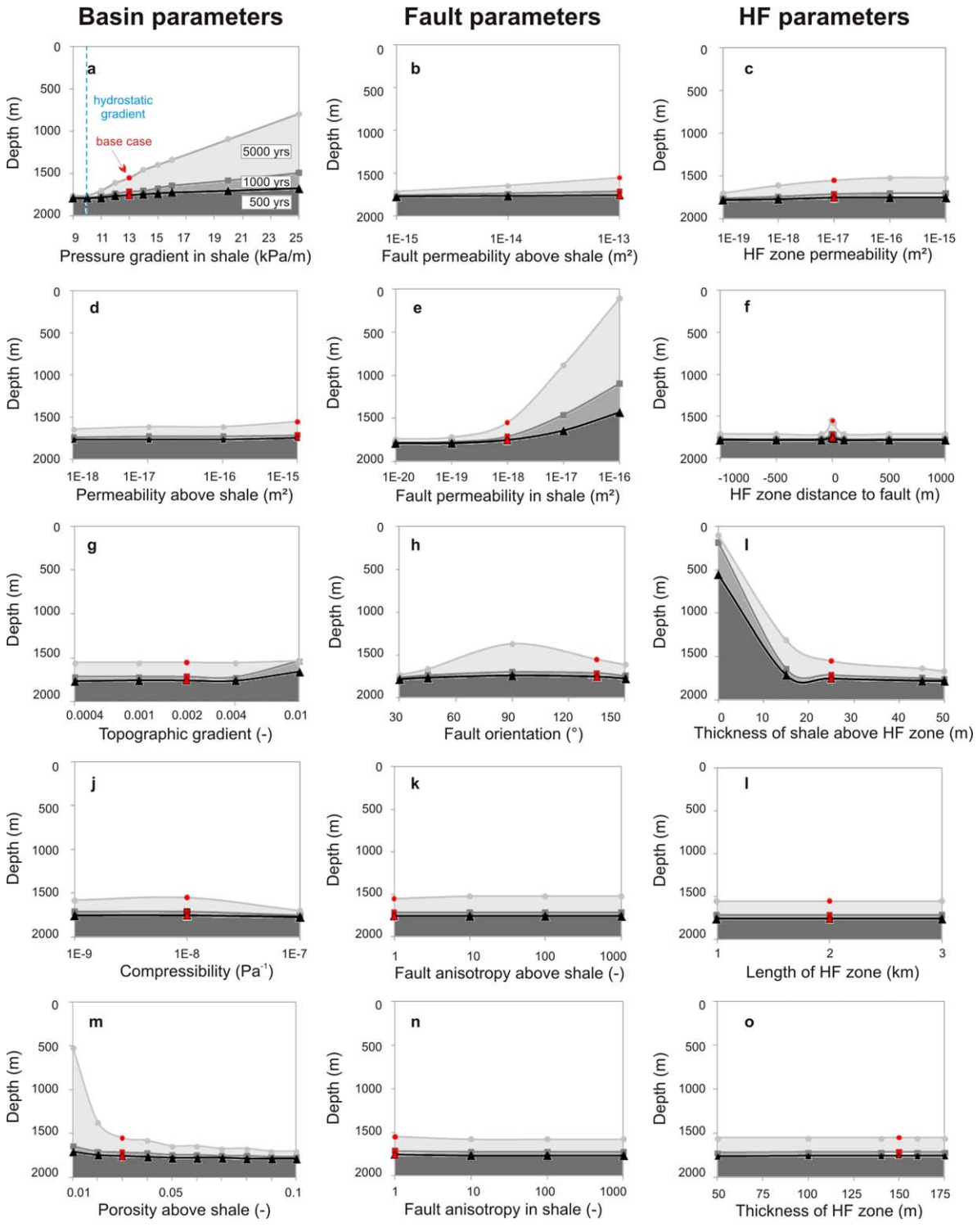

Figure 8. Sensitivity analysis with hydraulic fracturing (HF) in the middle of the shale. Depth relative to the land surface of potential contamination from the shale tracer depending on: (a) pressure gradient in shale; (b) fault permeability above shale; (c) HF zone permeability; (d) permeability above shale; (e) fault permeability in shale; (f) hydraulic fracturing (HF) zone distance to fault; (g) topographic gradient; (h) fault orientation; (i) thickness of shale above HF zone; (j) matrix compressibility; and (k) fault anisotropy above shale. Fault anisotropy is defined as the ratio of permeability along fault to permeability perpendicular to fault; (l) length of HF zone; (m) porosity above shale; (n) fault anisotropy in shale; and (o) thickness of HF zone. The lines and shading show the depth of potential contamination of a shale tracer relative concentration of 1% at $t = 500$ years (black), $t = 1000$ years (dark gray), and $t = 5000$ years (light gray). The base case scenario with hydraulic fracturing in the middle of the shale is shown in red circles.

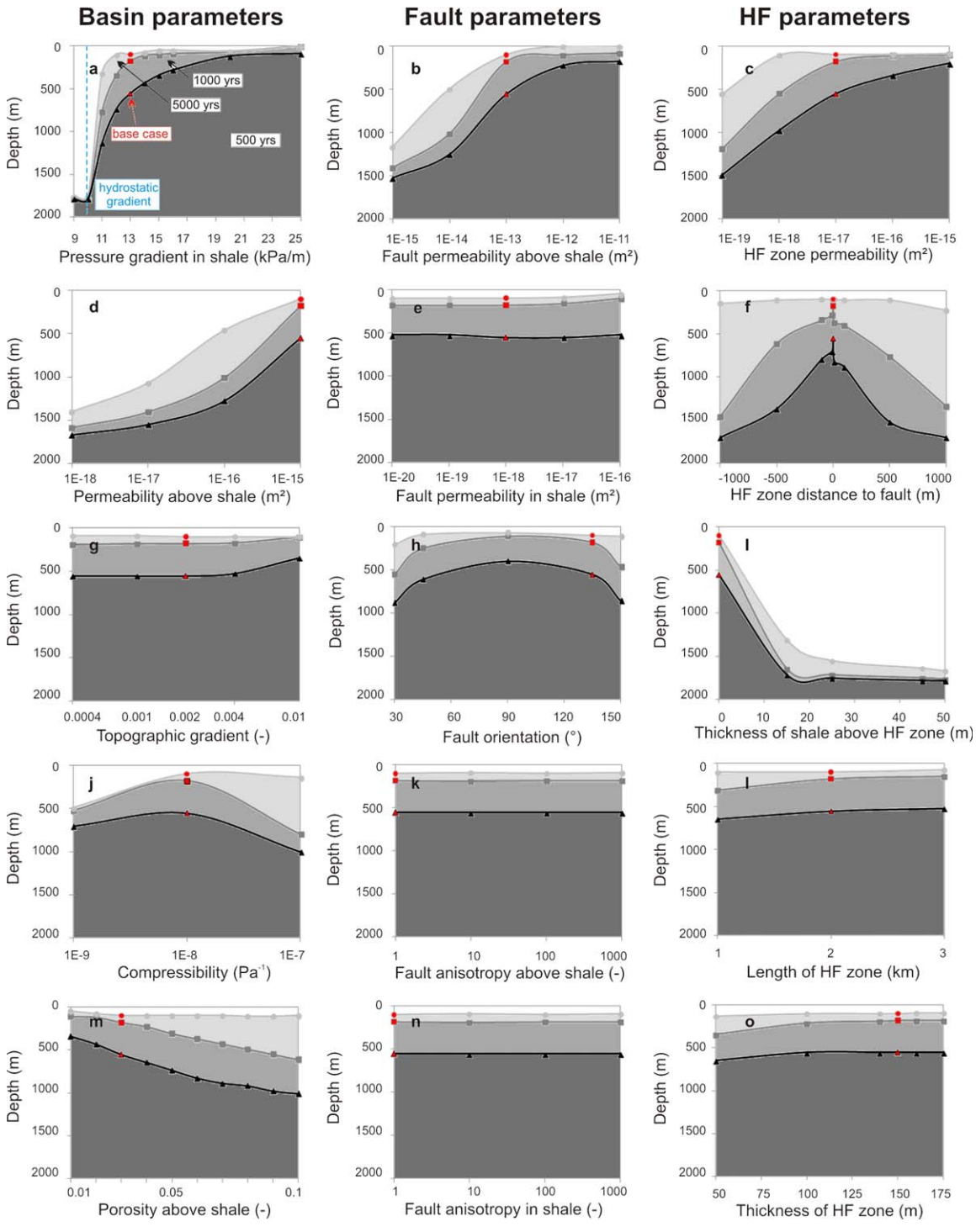

Figure 9. Sensitivity analysis with hydraulic fracturing (HF) at the top of the shale. Depth relative to the land surface of potential contamination from the shale tracer depending on: (a) pressure gradient in shale; (b) fault permeability above shale; (c) hydraulic fracturing (HF) zone permeability; (d) permeability above shale; (e) fault permeability in shale; (f) HF zone distance to fault; (g) topographic gradient; (h) fault orientation; (i) thickness of shale above HF zone; (j) matrix compressibility; and (k) fault anisotropy above shale. Fault anisotropy is defined as the ratio of permeability along fault to permeability perpendicular to fault; (l) length of HF zone; (m) porosity above shale; (n) fault anisotropy in shale; and (o) thickness of HF zone. The lines and shading show the depth of potential contamination of a shale tracer relative concentration of 1% at $t = 500$ years (black), $t = 1000$ years (dark gray), and $t = 5000$ years (light gray). The base case scenario with hydraulic fracturing at the top of the shale is shown in red circles.

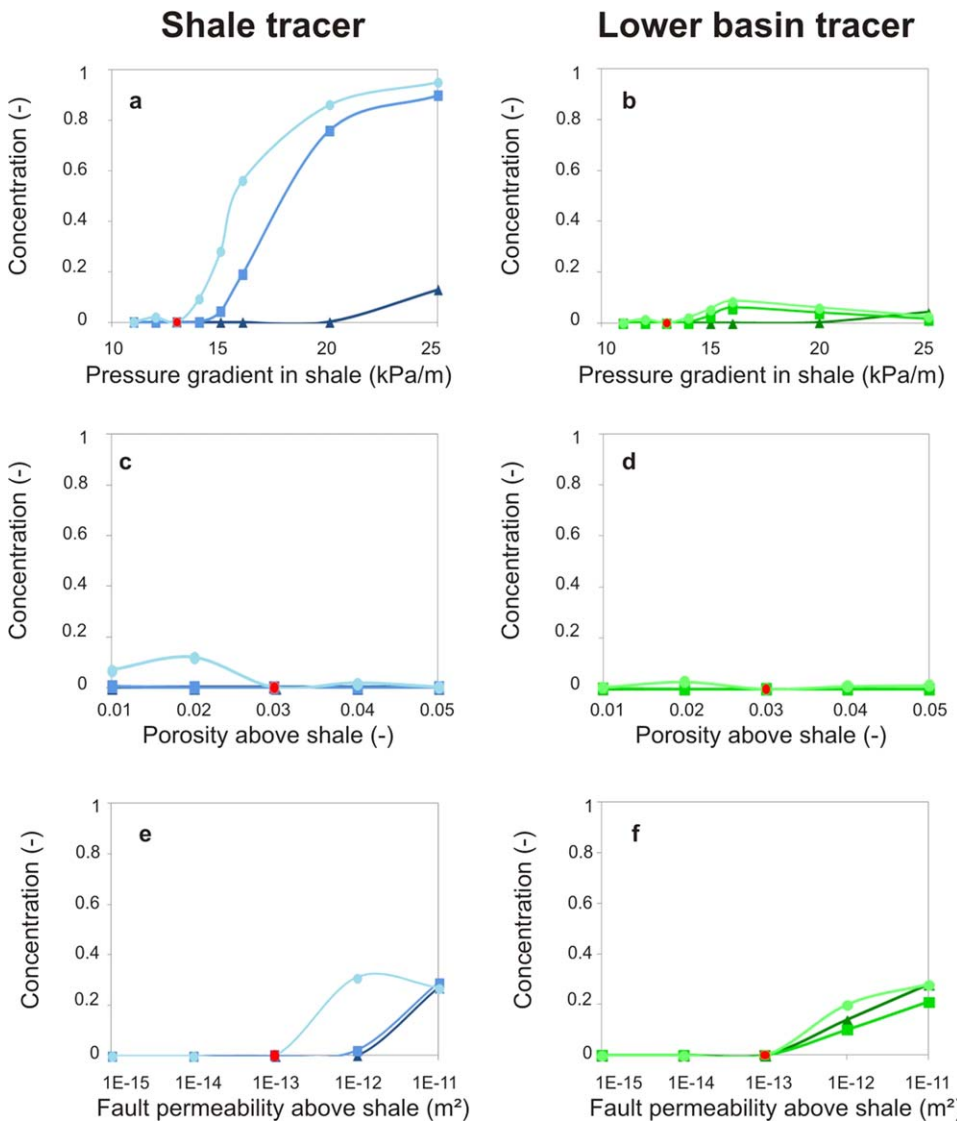

Figure 10. Concentrations at the base of the shallow aquifer. Concentration of (a, c, e, g, i) shale tracer and (b, d, f, h, j) lower basin tracer at the top of the fault following hydraulic fracturing at the top of the shale for several values of (a and b) pressure gradient in shale; (c and d) porosity above shale; (e and f) fault permeability above shale; (g and h) fault orientation; and (i and j) hydrofractured zone permeability. The lines show the depth of concentration of the shale (blue) or lower basin (green) tracer at the top of the fault at $t = 500$ years (dark blue, dark green), $t = 1000$ years (blue, green), and $t = 5000$ years (light blue, light green). The base case scenario with hydraulic fracturing at the top of the shale is shown in red circles.

[32] Numerical simulations show that fluid flow and contaminant transport potential is significantly enhanced when the hydrofractured zone is near the top of the shale unit (Figure 8i). Most shale formations are very thin; almost 30% of shale gas formations in the US are less than 50 m thick, and more than 60% of shale gas formations in the US are less than 100 m thick [*EIA*, 2011b]. It is thus technically and economically difficult to preserve intact shale over tens of meters above the hydraulically fractured zone. Hydraulic fracturing near the top of a gas shale unit is thus a realistic scenario. Similarly, fracturing of the overlying formations is generally avoided but has been reported [*Arkadakskiy and Rostron*, 2013]. Operators use microseismic monitoring to verify that hydraulic fracturing is restricted the shale gas unit. However, seismic monitoring was conducted in only about 3% of the hydraulic fracturing stages performed in the United States in 2009 [*Zoback et al.*, 2010]. It is thus difficult to evaluate how often the hydrofractured zone extends above the target formation. Although we did not simulate fracturing of the overlying formation, it is likely that this would highly increase the migration potential of contaminants along a fault according to the simulation results reported in this paper.

[33] In the case of hydraulic fracturing at the top of the shale, another crucial parameter controlling contaminant transport potential is the distance of the hydrofractured zone relative to the fault. Results show that with hydraulic fracturing at the top of the shale, migration rates greatly decrease for hydrofractured zones located from 500 to 1000 m away from the fault zone (Figure 9f). The average

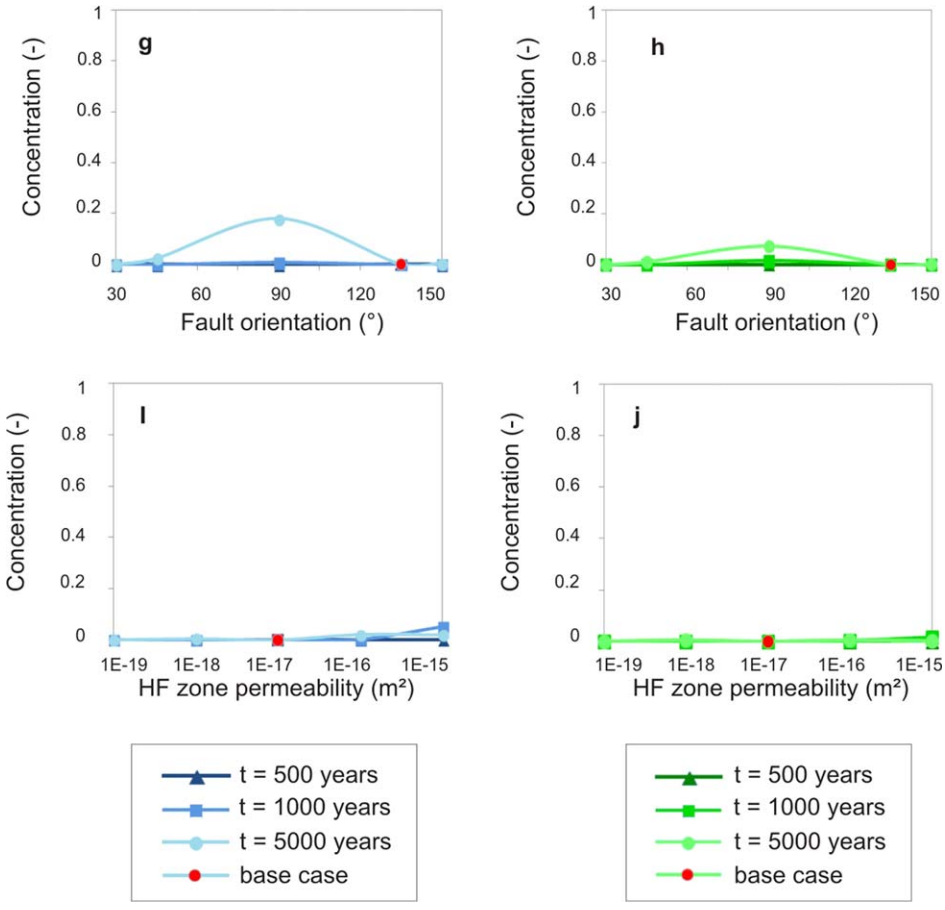

Figure 10. (continued)

distance between major faults is ∼6.6 km in the St. Lawrence lowlands [*Séjourné et al*., 2013] and horizontal wells are usually 1–3 km long [*Rivard et al*., 2012]. Regulations on well density and length as well as designing hydraulic fracturing zones a safe distance away from potentially conductive faults could greatly reduce the risk of groundwater contamination over long time scales due to migration via faults, although this assumes the three-dimensional distribution of faults zones is well defined and that the hydraulic properties of the fault zones is robustly characterized, with data publicly available for regulators and others to evaluate.

[34] Finally, basin and fault properties impact the migration potential. Numerical simulations show that matrix permeability and fault permeability in the overlying sediments highly affect the risk of contamination at shallow depths (Figures 9b and 9d). Additionally, pressure gradients within the shale are critical, as overpressured shales cause the upwards migration of contaminants, whereas migration rates are greatly reduced in hydrostatic and underpressured shales (Figure 9a). These basin and fault properties greatly vary between shale gas formations, and even potentially between faults within a basin, so knowledge of regional geologic, structural, and hydraulic properties would allow an initial assessment of contamination potential for a specific shale gas development. Depth to shale formation is also variable (500 m to 4.5 km in the United States) [*EIA*, 2011b]. Although we conducted simulations for a single value of depth to shale formation only (1.8 km), aquifer contamination should be more likely and rapid for shale formations at shallower depths.

[35] Simulation results show that for the base case scenario with hydraulic fracturing at the top of the shale, the extent of concentrations of shale tracer or lower basin tracer higher than 0.01 (1%) in the active zone is a few hundred meters, the extent of concentrations higher than 0.001 (0.1%) is ∼1 km, and maximum concentrations of the shale tracer and lower basin tracer in the shallow aquifer are 5% (Figure 6). However, values of relative concentrations and extent of plume in the shallow aquifer should be used with caution, as they depend on the density of contaminants and the lateral groundwater velocities in the active zone, which are not the focus of this study. Values of concentration at the base of the shallow aquifer (at the top of the fault) are more reliable. Simulations show that almost full concentration of the shale tracer and mass fluxes up to 10 kg/yr/m of TDS could reach the shallow aquifer under high pressure gradients in the shale, indicating that the impact on groundwater quality could be quite important (Figures 10a and 11).

[36] The results from this study are, in part, limited by some aspects of the numerical model used in this study:

[37] 1. We simulate single-phase flow, whereas shale formations contain gas, water, and sometimes oil. To better describe the migration of the gas phase, one should consider gas carried in solution by oil, gas carried in solution by water, and gas movement as a separate phase. In multiphase flow, buoyancy and capillary forces would impact

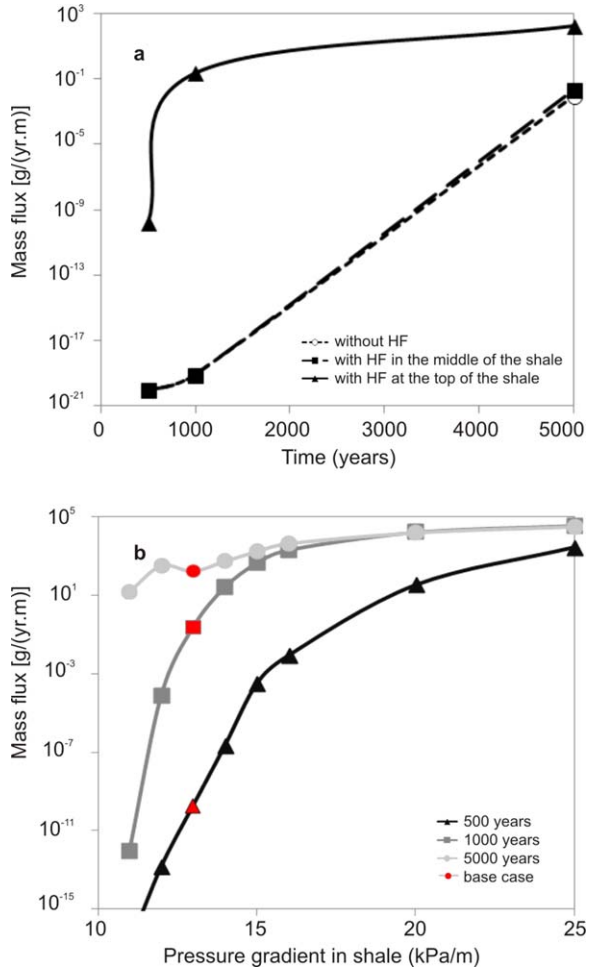

Figure 11. Comparison of the mass flux at the top of the fault against time and the pressure gradient in the shale. The fluxes were calculated by assuming the tracer in the shale and lower basin (at the top of the fault) had an initial concentration of TDS of 100 kg/m^3. (a) Mass flux through time for the three simulations shown in Figure 5 without hydraulic fracturing, with hydraulic fracturing in the middle of the shale and at the top of the shale and (b) mass flux with hydraulic fracturing under several pressure gradients in shale.

fluid flow by their opposite, competing effects [*Ingebritsen et al*., 2006]. The buoyancy force would increase the potential for contaminant migration, whereas capillary forces would decrease it. Furthermore, single-phase models do not describe the dynamic relationships between storage, permeability, and water content of the shale and overlying units that contain gas and are thus only partially saturated with water. Further work is needed to assess the impact of multiphase flow on this migration pattern.

[38] 2. We use a 2D cross-sectional model which implies the conditions of an infinitely extended fault and hydrofractured zone in the third dimension.

[39] 3. We simulate the impact of hydraulic fracturing by a change in permeability, without considering the pressure regime in the well during and after hydraulic fracturing operations. This is justified by the long-term simulation over several thousand years, long after gas well closure. However, we acknowledge that it could impact migration of contaminants in the first years to decades of shale gas extraction.

[40] 4. Initial pressure propagation associated with hydraulic fracturing was neglected as recent work suggests that the pressure perturbation is likely to be restricted to the vicinity of the hydraulic fractures [*Flewelling and Sharma*, 2013]. If pressure disturbances due to hydraulic fracturing persist for several years and affect an important volume of the formation, the upward transport of fluid could be accelerated.

[41] 5. We consider a stable sedimentary basin with generally low thermal gradient and simulate isothermal conditions. High thermal gradients would reduce the water density, which would enhance upward flow assuming permeability was large enough for buoyancy driven flow [*Ingebritsen et al*., 2006].

[42] 6. We consider regional faults, which may or may not be precisely located in 3D at the depth of shale gas formations.

[43] 7. In some simulations, we assume that the hydrofractured zone extends to the top of the shale over its entire length. However, in multistage fracturing, the first stages allow for adjusting the additional fracturing. A first stage of fracturing showing fluid losses due to connectivity with the zone above the shale unit would likely be corrected during the additional stages of hydraulic fracturing operations.

[44] 8. We assume that the hydrofractured zone and the fault zone have persistent high permeabilities. We acknowledge that fractures may close over the modeled time period, which would lead to a decrease in permeability and reduce the upwards migration of contaminants.

[45] 9. We do not account for production and extraction of shale gas and associated fluids, which would lower the pressure in the hydrofractured zone and decrease the initial upward mobility of solutes, as well as the duration of overpressured conditions that drive upward fluid flow.

[46] 10. A change in the initial distribution of salinity could impact the time of migration of contaminants, as a lower density would enhance upwards flow and a higher density would decrease it.

[47] 11. Recharge rates used in this study are lower by approximately an order of magnitude compared to the ones present in the St. Lawrence lowlands, and may be more representative of more arid regions. A higher recharge rate would lower the concentrations of solutes in the aquifer, but would not impact the results in terms of solute mass fluxes reaching the freshwater aquifer.

[48] Long-term risk of groundwater contamination due to migration via faults raises the question of the appropriate time frame of water management, especially when dealing with large-scale industrial activities with potential cumulative effects such as shale gas development. The time frame of water resources management is typically 5–20 years [*Gleeson et al*., 2012], which may be appropriate for surface water systems which have short residence times. However, groundwater can have very long residence times. The global average groundwater residence time is estimated to be 1400 years [*UNESCO*, 1978]. Geological repositories for high-level nuclear waste are designed to limit escape to the biosphere tens to hundreds of thousands of years. A multigenerational time horizon of 50–100 years for the management of groundwater has been proposed by *Gleeson et al*. [2012], so that the impacts of a broad range of hydrogeological conditions can be adequately built into effective management and policy plans. *Lenton* [2011] suggested an even longer time horizon of 1000 years as a full, ethical time horizon for which the

human impact on biophysical systems should be evaluated. Monitoring over this time-frame and the precautionary principle [*Norton*, 2005] would be especially appropriate for deep sedimentary basins, such as those where shale gas is found, where at least some part of the exploited groundwater resources have a very long residence time and the impact of contamination at depth is likely irreversible.

6. Conclusions

[49] Publically available data of shale gas basins and hydraulic fracturing operations were systematically compiled to serve as a basis for the development of a two-dimensional model of a generic, regional, faulted sedimentary basin having an active groundwater flow zone at its upper limit. Hydraulic fracturing was represented in the model by a change in permeability and simulations investigated its potential impact on fluid flow and contaminant transport from the shale formation to a shallow aquifer along a fault zone. A sensitivity analysis was carried out to identify which parameters control the contaminant transport potential.

[50] Contamination from the target shale unit to shallow aquifers due to hydraulic fracturing is often neglected [*Arthur et al*., 2008; *Zoback et al*., 2010; *BAPE*, 2011; *Howarth et al*., 2011; *Osborn et al*., 2011; *EPA*, 2012]. However, numerical simulation results from this study show that migration of contaminants along a fault zone to shallow depths could occur under some specific conditions. Although simulation results show that contamination occurs on long timescales (∼1000 years), this scenario of contamination should not be ignored, but should rather be further investigated. This study raises the question of the time frame of water resources management and the ethical time frame to be considered when actions are taken to prevent groundwater contamination. Results show that the most important parameter controlling contaminant transport potential is the location of the hydro-fractured zone relative to the fault zone and fracturing of the top of the shale, suggesting that contamination via permeable faults could be prevented if regional faults are mapped and avoided. Upward migration of contaminants also has to be driven by an overpressure in the shale unit. Basin and fault parameters, such as matrix and fault permeability in the overlying sediments also impact migration potential.

[51] Further work is needed to assess potential upwards migration along a fault zone following gas shale hydraulic fracturing. Numerical simulations, including multiphase flow, would allow a better description of hydrological processes in the shale, fault, and overlying formations. Additional data from hydraulic fracturing operations, such as pressure regime and variation in permeability during hydraulic fracturing, should be recorded and made publically available as they would be highly valuable in order to develop numerical models that are as realistic as possible. Before hydraulic fracturing operations, hydrogeological properties of the subsurface and faults location, density and hydraulic properties should be analyzed in order to evaluate the risk of shallow groundwater contamination by migration via fault zones. The precautionary principle [*Norton*, 2005] suggests hydraulic fracturing should not be carried out near potentially conductive faults, and that regulations should consider monitoring the contamination potential due to migration via faults over longer timespans than water resources management typically consider.

[52] **Acknowledgments.** Discussions with V. Bense improved this paper. Thorough and constructive reviews by S. Ge and two anonymous reviewers lead to significant improvements of the paper. NSERC and FQRNT Projet de recherche en équipe supported this collaborative research. TG was also supported by a Global Fellowship from the Canadian Institute for Advanced Research.

References

Alpha Environmental Consultants, I. (2009), Technical consulting reports prepared in support of the draft supplemental generic environmenal impact statement for natural gas production in New York state, Report, New York State Energy Research and Development Authority, Albany, N. Y.

Arkadakskiy, S., and B. Rostron (2013), Tracking out-of-zone hydraulic fracturing in the Bakken with naturally occuring tracers, *GeoConvention* 2013, 2013 CSEG, CSPG CWLS Joint Convention, Calgary, May 6-10, 2013.

Arthur, J., B. Bohm, and M. Layne (2008), Hydraulic fracturing considerations for natural gas wells of the Marcellus Shale, in *The Ground Water Protection Council Annual Meeting,* Cincinnati, Ohio.

Aydin, A. (2000), Fractures, faults, and hydrocarbon entrapment, migration and flow, *Mar. Pet. Geol.*, *17*(7), 797–814.

BAPE (2011), Développement durable de l'industrie des gaz de schiste au Québec, Report, 336 pp, Bureau d'audiences publiques sur l'environnement, Que.

Bense, V. F., and M. A. Person (2006), Faults as conduit-barrier systems to fluid flow in siliciclastic sedimentary aquifers, *Water Resour. Res.*, *42*, W05421, doi:10.1029/2005WR004480.

Bense, V. F., T. Gleeson, S. E. Loveless, O. Bour, and J. Scibek (2013), Fault zone hydrogeology, *Earth Science Reviews*, doi:10.1016/j.earscirev.2013.09.008.

Björlykke, K., and K. Gran (1994), Salinity variations in North Sea formation waters: Implications for large-scale fluid movements, *Mar. Pet. Geol.*, *11*(1), 5–9.

Boles, J. R., P. Eichhubl, G. Garven, and J. Chen (2004), Evolution of a hydrocarbon migration pathway along basin-bounding faults: Evidence from fault cement, *AAPG Bull.*, *88*(7), 947–970.

Caine, J. S., J. P. Evans, and C. B. Forster (1996), Fault zone architecture and permeability structure, *Geology*, *24*(11), 1025–1028.

Childs, C., T. Manzocchi, J. J. Walsh, C. G. Bonson, A. Nicol, and M. P. J. Schöpfer (2009), A geometric model of fault zone and fault rock thickness variations, *J. Struct. Geol.*, *31*(2), 117–127.

Cipolla, C., S. Maxwell, M. Mack, and R. Downie (2011), A practical guide to interpreting microseismic measurements, in *North American Unconventional Gas Conference and Exhibition*, eiited by SPE, pp. 1–28, Soc. of Pet. Eng., The Woodlands, Tex.

Cohen, H. A., T. Parratt, and C. B. Andrews (2013), Potential contaminant pathways from hydraulically fractured shale to aquifers, *Groundwater*, *51*(3), 317–319.

Connolly, C., L. Walter, H. Baadsgaard, and F. Longstaffe (1990), Origin and evolution of formation waters, Alberta basin, western Canada sedimentary basin. I. Chemistry, *Appl. Geochem.*, *5*(4), 375–395.

Davies, R., S. Mathias, J. Moss, S. Hustoft, and L. Newport (2012), Hydraulic fractures: How far can they go?, *Mar. Pet. Geol.*, *37*, 1–6.

EIA (2011a), World shale gas resources: An initial assessment of 14 regions outside the United States, Report, 365 pp., U.S. Dep. of Energy, Washington, D. C.

EIA (2011b), Review of emerging resources: U.S. shale gas and shale oil plays, Report, 105 pp., U.S. Dep. of Energy, Washington, D. C.

EPA (2012), Study of the potential impacts of hydraulic fracturing on drinking water resources: Progress report, Report, United States Environmental Protection Agency, Washington, D. C.

Faulkner, D., C. Jackson, R. Lunn, R. Schlische, Z. Shipton, C. Wibberley, and M. Withjack (2010), A review of recent developments concerning the structure, mechanics and fluid flow properties of fault zones, *J. Struct. Geol.*, *32*(11), 1557–1575.

Flewelling, S. A., and M. Sharma (2013), Constraints on upward migration of hydraulic fracturing fluid and brine, *Groundwater*, 29 July 2013, 11 pp., doi: 10.1111/gwat.12095.

Freeze, R. A., and J. A. Cherry (1979), *Groundwater*, 604 pp., Prentice Hall, Eaglewood Cliffs, N. J.

Garven, G. (1995), Continental-scale groundwater flow and geologic processes, *Annu. Rev. Earth Planet. Sci.*, *23*, 89–117.

Gleeson, T., W. M. Alley, D. M. Allen, M. A. Sophocleous, Y. Zhou, M. Taniguchi, and J. VanderSteen (2012), Towards sustainable groundwater use: setting long-term goals, backcasting, and managing adaptively, *Ground Water*, *50*(1), 19–26.

Gleeson, T., L. Smith, N. Moosdorf, J. Hartmann, H. H. Dürr, A. H. Manning, L. P. H. van Beek, and A. M. Jellinek (2011), Mapping permeability over the surface of the Earth, *Geophys. Res. Lett.*, *38*, L02401, doi:10.1029/2010GL045565.

Globensky, Y. (1972), Gaz-Pétrole-Eau salée dans les puits forés au Québec entre 1860 et 1970.

Gregory, K., R. Vidic, and D. Dzombak (2001), Water management challenges associated with the production of shale gas by hydraulic fracturing, *Elements*, *7*, 181–186.

Gregory, K. B., R. D. Vidic, and D. A. Dzombak (2011), Water management challenges associated with the production of shale gas by hydraulic fracturing, *Elements*, *7*(3), 181–186.

Groundwater Protection Council, and All Consulting (2009), Modern shale gas development in the United States: A primer, Report, 116 pp., U.S. Dep. of Energy, Office of Fossil Energy, Washington, D. C.

Hanor, J., and J. McIntosh (2007), Diverse origins and timing of formation of basinal brines in the Gulf of Mexico sedimentary basin, *Geofluids*, *7*(2), 227–237.

Howarth, R., A. Ingraffea, and T. Engelder (2011), Natural gas: Should fracking stop?, *Nature*, *477*(7364), 271–275.

Hughes, J., and W. Sanford (2005), SUTRA-MS a version of SUTRA modified to simulate heat and multiple-solute transport, Report, 141 pp., *U.S. Geol. Surv. Open-File Rep. 2004-1207*, Reston, Virginia.

Ingebritsen, S. E., W. E. Sanford, and C. E. Neuzil (2006), *Groundwater in Geological Processes*, 562 pp., Cambridge Univ. Press, New York, N. Y.

Kargbo, D. M., R. G. Wilhelm, and D. J. Campbell (2010), Natural gas plays in the Marcellus Shale: Challenges and potential opportunities, *Environ. Sci. Technol.*, *44*(15), 5679–5684.

Kharaka, Y. K., and J. J. Thordsen (1992), Stable isotope geochemistry and origin of waters in sedimentary basins, in *Isotopic Signatures and Sedimentary Records*, edited by Clauer, N., S. Chaudhuri, pp. 411–466, Springer, Berlin Heidelberg.

King, G. (2012), Hydraulic Fracturing 101: What every representative, environmentalist, regulator, reporter, investor, university researcher, neighbor and engineer should know about estimating frac risk and improving frac performance in unconventional gas and oil wells, paper presented at SPE Hydraulic Fracturing Technology Conference. Society of Petroleum Engineers, 6–8 February, The Woodlands, Tex.

Konstantinovskaya, E., M. Malo, and D. A. Castillo (2012), Present-day stress analysis of the St. Lawrence Lowlands sedimentary basin (Canada) and implications for caprock integrity during CO2 injection operations, *Tectonophysics*, *518–521*, 119–137.

Lavoie, D., A. Hamblin, R. Thériault, J. Beaulieu, and D. Kirkwood (2008), The Upper Ordovician Utica Shales and Lorraine Group flysch in southern Québec: Tectonostratigraphic setting and significance for unconventional gas, Report, Geol. Surv. of Canada, GSC Open File 5900, Ottawa, Ontario.

Lenton, T. (2011), Early warning of climate tipping points, *Nat. Clim. Change*, *1*(4), 201–209.

Lombardi, S., and D. Pinti (1992), Rn-222 behavior at the Latera geothermal field (Northern Latium, Italy), *J. Radioanal. Nucl. Chem.*, *161*(2), 365–375.

Maxwell, S., M. Jones, R. Parker, S. Miong, S. Leaney, D. Dorval, D. D'Amico, J. Logel, E. Anderson, and K. Hammermaster (2009), Fault activation during hydraulic fracturing., in *SEG Technical Program*, pp. 1552–1556. Society of Exploration Geophysicists (SEG), Houston 2009 Annual Meeting, Houston, Texas, USA, October 27-29, 2009.

Montgomery, S., D. Jarvie, K. Bowker, and R. Pollastro (2005), Mississippian Barnett Shale, Fort Worth basin, north-central Texas: Gas-shale play with multi-trillion cubic foot potential, *AAPG Bull.*, *89*(2), 155–175.

Moretti, I. (1998), The role of faults in hydrocarbon migration, *Pet. Geosci.*, *4*(1), 81–94.

Muchez, P., W. Heijlen, D. Banks, D. Blundell, M. Boni, and F. Grandia (2005), 7: Extensional tectonics and the timing and formation of basin-hosted deposits in Europe, *Ore Geol. Rev.*, *27*(1–4), 241–267.

Myers, T. (2012), Potential contaminant pathways from hydraulically fractured shale to aquifers, *Ground Water*, *50*(6), 872–882.

Nacht, P., M. De Oliveira, D. Roehla, and A. Costa (2012), Investigation of geological fault reactivation and opening, *Mecánica Computacional*, *XXIX*, 8687–8697.

Neuzil, C. E. (1994), How permeable are clays and shales?, *Water Resour. Res.*, *30*, 145–150.

Tran Ngoc, T. D., E. Konstantinovskaya, R. Lefebvre, M. Malo, and L. Massé (2011), Geotechnical characterization of deep saline aquifers for CO_2 geological storage in the Bécancour region, Québec, Canada, in *Geotechnics for Sustainable Development*, edited by D. L. Phung, Construction Publishing House, Hanoi.

Norton, B. G. (2005), *Sustainability : A Philosophy of Adaptive Ecosystem Management*, 607 pp., University of Chicago Press, Chicago, Ill.

Osborn, S. G., A. Vengosh, N. R. Warner, and R. B. Jackson (2011), Methane contamination of drinking water accompanying gas-well drilling and hydraulic fracturing, *Proc. Natl. Acad. Sci. U. S. A.*, *108*(20), 8172–8176.

Person, M., A. Banerjee, A. Hofstra, D. Sweetkind, and Y. Gao (2008), Hydrologic models of modern and fossil geothermal systems in the Great Basin: Genetic implications for epithermal Au-Ag and Carlin-type gold deposits, *Geosphere*, *4*(5), 888–917.

Person, M. A., J. P. Raffensperger, S. Ge, and G. Garven (1996), Basin-scale hydrogeologic modeling, *Rev. Geophys.*, *34*(1), 61–87.

Pfaff, K., L. Hildebrandt, D. Leach, D. Jacob, and G. Markl (2010), Formation of the Wiesloch Mississippi Valley-type Zn-Pb-Ag deposit in the extensional setting of the Upper Rhinegraben, SW Germany, *Miner. Deposita*, *45*(7), 647–666.

Pinti, D., and B. Marty (2000), Noble gases in oil and gas fields: origins and processes, in *Fluids Basin Evolution*, edited by K. Kyser, *Mineral. Assoc. Can. Short Course*, *28*, 160–196.

Rawling, G. C., L. B. Goodwin, and J. L. Wilson (2001), Internal architecture, permeability and hydrologic significance of contrasting fault-zone types, *Geology*, *29*(1), 43–46.

Rivard, C., J. Molson, D. Soeder, E. Johnson, S. Grasby, B. Wang, and A. Rivera (2012), A review of the November 24–25, 2011 shale gas workshop, Calgary, Alberta—2. Groundwater resources, Report, Geol. Surv. of Canada, GSC Open File 7096, 205 pp., doi:10.4095/290257.

Rudnicki, J. (2002), Alteration of regional stress by reservoirs and other inhomogeneities: Stabilizing or destabilizing?, in *Proceedings of the Ninth International Congress on Rock Mechanics*, edited by G. Vouille and P. Berest, 25–28 Aug, vol. 3, pp. 1629–1637, Paris, France.

Saiers, J., and E. Barth (2012), Potential contaminant pathways from hydraulically fractured shale aquifers, *Ground Water*, *50*(6), 826–828.

Séjourné, S., X. Malet, R. Lefebvre, and D. Lavoie (2013), Synthèse hydrogéologique du Shale d'Utica et des unités sus-jacentes (Lorraine, Queenston et dépôts meubles), Basses-Terres du Saint-Laurent, Québec, Report, Geol. Surv. of Canada.

Sibson, R. (1990), Faulting and fluid flow, in *Short Course on Fluids in Tectonically Active Regions of the Continental Crust*, edited by B. E. Nesbitt, *Mineral. Assoc. of Canada Handbook*, pp. 93–132, Quebec, Canada.

Soeder, D. (1988), Porosity and permeability of easter devonian gas shale, *SPE Form Eval.*, *3*(1), 116–124.

Soltanzadeh, H., and C. Hawkes (2008), Semi-analytical models for stress change and fault reactivation induced by reservoir production and injection, *J. Pet. Sci. Eng.*, *60*(2), 71–85.

Soltanzadeh, H., and C. Hawkes (2009), Assessing fault reactivation tendency within and surrounding porous reservoirs during fluid production or injection, *Int. J. Rock Mech. Min. Sci.*, *46*(1), 1–7.

Streit, E., and R. Hillis (2004), Estimating fault stability and sustainable fluid pressures for underground storage of CO2 in porous rock, *Energy*, *29*(9–10), 1445–1456.

Sumi, L. (2008), Shale gas: Focus on the marcellus shale, Report, The Oil and gas accountability project/Earthworks, Durango, Colo.

Tóth, J. (1963), A theoretical analysis of groundwater flow in small drainage basins, *J. Geophys. Res.*, *68*(16), 4795–4812.

UNESCO (1978), *World Water Balance and Water Resources of the Earth*, 663 pp., UNESCO, Paris.

Voss, C., and A. Provost (2002), SUTRA, A model for saturated-unsaturated variable-density ground-water flow with solute or energy transport, *U.S. Geol. Surv. Water Resour. Invest. Rep*. 02-4231, Reston, VA.

Wessels, S., A. De La Peña, M. Kratz, S. Williams-Stroud, and T. Jbeili (2011), Identifying faults and fractures in unconventional reservoirs through microseismic monitoring, *First Break*, *29*, 99–104.

Yielding, G., B. Freeman, and D. Needham (1997), Quantitative fault seal prediction, *AAPG Bull.*, *81*(6), 897–917.

Zoback, M. D. (2007), *Reservoir Geomechanics*, 449 pp., Cambridge Univ. Press, N. Y.

Zoback, M., S. Kitasei, and B. Copithorne (2010), Addressing the environmental risks from shale gas development, Report, 365 pp, Worldwatch Institute, U.S. Dep. of Energy, Washington, D. C.